Observation and Manipulation of the Wave Nature of Phonon Thermal Transport through Superlattices

by

Maria N. Luckyanova

B.S. Department of Mechanical Engineering, Massachusetts Institute of Technology (2008)
S.M. Department of Mechanical Engineering, Massachusetts Institute of Technology (2012)

Submitted to the Department of Mechanical Engineering
in partial fulfillment of the requirements for the degree of

Doctor of Philosophy in Mechanical Engineering

at the

MASSACHUSETTS INSTITUTE OF TECHNOLOGY

September 2015

Author .... Signature redacted ....
Department of Mechanical Engineering
August 20, 2015

Certified by.... Signature redacted ....
Gang Chen
Carl Richard Soderberg Professor of Power Engineering
Thesis Supervisor

Accepted by .... Signature redacted ....
David E. Hardt
Chairman of the Committee on Graduate Students

Observation and Manipulation of the Wave Nature of Phonon Thermal Transport through Superlattices

by

Maria N. Luckyanova

Submitted to the Department of Mechanical Engineering
on August 20, 2015, in partial fulfillment of the
requirements for the degree of
Doctor of Philosophy in Mechanical Engineering

Abstract

As the scale of electronic, photonic, and energy harvesting devices has shrunk, the importance of understanding nanoscale thermal transport has grown. In this thesis, we investigate thermal transport through superlattices (SLs), periodic layers of thin films, to better understand thermal conduction at these small scales. The classical picture of nanoscale thermal transport invokes a picture of diffusive scattering of phonons, or lattice vibrations, at the interfaces and boundaries in structures. This picture has been used to explain experimental thermal transport results for a wide variety of nanostructures. Despite the omnipresence of this particle-transport picture of phonon heat conduction, the community has continuously sought an experimental demonstration of the wave regime of thermal transport in nanostructures.

In this thesis, we report the first experimental observations of the regimes of coherent phonon transport and phonon localization in thermal conduction through nanostructures. First, in order to better understand thermal transport through SLs, we present measurements of anisotropic thermal conductivity in the same GaAs/AlAs SLs using two different optical techniques, time-domain thermoreflectance (TDTR) for cross-plane measurements, and transient thermal grating (TTG) for in-plane measurements. The results of this study lend insight into the role of interface scattering, previously understood to be the dominant scattering mechanism in these structures, in SLs. The experimentally measured thermal conductivities are compared to results from first principles simulations, and the agreement between the two helps to validate atomistic simulation techniques of transport through SLs.

The role of coherent phonon transport is explored by using the TDTR technique to measure the thermal conductivities of SLs with the same period thicknesses but varying numbers of periods. This experimental approach is a departure from traditional studies of SLs where period thicknesses are varied while the SL is grown to be thermally thick. This shift in the experimental paradigm allows us to explore previously elusive phenomena in nanoscale thermal transport. Combined with first principles and Green's functions simulations, the results of these experiments are the first experimental observation of coherent phonon transport through SLs.

Finally, experiments on GaAs/AlAs SLs with varying concentrations of ErAs nanodots at the interfaces show the ability to destroy this phonon coherence. The thermal conductivities of such SLs with constant period thicknesses and varying numbers of periods show an overall reduction in thermal conductivity with increasing ErAs concentration. In addition, at low temperatures samples with ErAs at the interfaces show a maximum in thermal conductivity with shorter sample length and then a drop-off for longer samples. These results are signatures of phonon localization, a previously unobserved thermal transport phenomenon.

Thesis Supervisor: Gang Chen
Title: Carl Richard Soderberg Professor of Power Engineering

Acknowledgments

During my many years at MIT, I have been lucky to meet, know, and work with many wonderful people. First and foremost on the list is Prof. Gang Chen. Gang is generous with his time, his knowledge, and the opportunities he gives his graduate students to grow as researchers and engineers. Though my successes waxed and waned, his support never did, and for that I owe him a large debt of gratitude. I am grateful to the other extraordinary faculty on my committee, Prof. Millie Dresselhaus, Prof. Keith A. Nelson, and Prof. Evelyn Wang. I was fortunate to work with them not only in the capacity of their comprising my committee, but in monthly S3TEC meetings. There they showed, by their example, what it was to work selflessly and relentlessly for the advancement of science. I would be remiss if I didn't also thank Prof. John G. Brisson who was my teacher and mentor and introduced me to the study of heat transfer when I was an undergraduate. Prof. Brisson's enthusiasm for teaching and enthusiasm for the subject were inspirations for me to continue my studies at MIT for what turned out to be eleven years.

To my peers in the NanoEngineering group at MIT, thank you for the kindness, and the spirit of collaboration and openness that is the foundation of our group. Sitting in the RK lab and overhearing the constant problem solving that occurs here, I am reminded on a daily basis how no man is an island when it comes to doing research. I want to especially thank Prof. Aaron Schmidt, Dr. Kim Collins, Dr. Austin Minnich, Dr. John Cuffe, Lingping Zeng, Bolin Liao, Samuel Huberman, Prof. Zhiting Tian, and Prof. Tengfei Luo, the constituents of nano-ttr@mit.edu. I also want to thank the other members of the NanoEngineering group that have made this experience so enjoyable: Prof. Sangyeop Lee, Dr. Ken McEnaney, Dr. Matthew Branham, Poetro Sambegoro, Daniel Kraemer, Jesse, Silvia, Jianjian Wang, James Loomis, Jonathan Tong, Wei-chun Hsu, and Lee Weinstein.

I am thankful to the National Science Foundation and the Department of Energy's Energy Frontier Research Center program for their generous financial support.

I am grateful to my parents, Dr. Olga Voronkova and Dr. Nick Luckyanov for their support and the emphasis they've placed on my education throughout my life. I am thankful to my myriad friends who have enriched my life so deeply and fully: Marianne, Katherine, Melis, Billy, Tess, Jess, Elysa, Dan, Scott, Jeff, Sara, Andrea, David, Will, Jonathan, Jesse+and+Silvia (and their kids, Alisa and Blooby), and Keith (and my other nieces, Katherine and Julia). Finally, I want to give a special thanks to my sweet sister, Natalia. Much of my identity is warmly wrapped up in being Natalia's little sister and the appreciation I have for having her in my life is boundless.

Contents

List of Figures

Chapter 1

Introduction

In 1807, building on the work of chemists, physicists, and mathematicians that came before him, Joseph Fourier submitted his work describing the relationship between an object's temperature and the heat passing through its boundaries, Théorie de la Propagation de la Chaleur dans les Solides (On the Propagation of Heat in Solid Bodies) to the Paris Institute. In the ensuing 15 years it engendered heated debate and consideration, ultimately ending in the publication of his seminal Théorie Analytique de la Chaleur (Analytic Theory of Heat) in 1822. Since the publication of this work, Fourier's mathematical description of diffusion has been adapted by a vast array of fields to describe processes chemical [1, 2], biological [3, 4], mechanical [5, 6, 7], mathematical [8], and electromagnetic [9, 10, 11]. In fact, Fourier came up with the equation bearing his name at a time when there was still much disagreement over whether heat was a weightless fluid moving through a body (caloric) or the miniscule motion of the unseeable atoms composing the body itself. Fourier got around this debate by considering an infinitesimally small but definable point as having a temperature and a heat content dependent only on the similarly definable points around it. In this way, he created his powerful differential equation,

$$\nabla \cdot k\nabla T = c\frac{\partial T}{\partial t}. \tag{1.1}$$

This equation says that the temperature, T, of an infinitesimally small but definable point changes in time as a function of the three-dimensional temperature gradient surrounding it, and two intrinsic material properties c, the specific heat capacity per unit volume and k, the thermal conductivity that describe how well the point can store and transport heat, respectively. The beauty of this relation is multidimensional, but of particular convenience is the fact that understanding the nature of heat is completely superfluous, giving both sides of the debate a relation that they could believe. Thus was born the theory of continuum heat conduction. This theory endured in describing thermal transport through solids for a century.

In 1938, however, W. J. de Haas and Th. Biermasz published two studies on the ultra-low-temperature thermal conductivities of KCl and SiO2 rods [12, 13]. They found, experimentally for the first time, that the thermal conductivity of these rods depended on their diameters. This was the first experimental result suggesting that thermal conductivity was not intrinsic, as Fourier believed it to be. This seemed to validate a suggestion put forth in 1929 by Rudolf Peierls that the boundaries of a finite sample will change the total resistance of the sample, appearing to lower its thermal conductivity due to the increased resistance [14]. Hendrik Casimir, examining both this Peierls theory and the experimental results of de Haas and Biermasz, came up with what became a long-standing theory explaining such a reduction in thermal conductivity [15]. Casimir employed a radiation analogy in his analysis to show that the reduction of the thermal conductivity for rods at low temperatures is due to a reduction in the distances that an oscillating wave of the lattice, or phonon (a name this oscillation only received in 1932 [16]) could travel and thus carry its energy. Since then, Casimir's picture of thermal transport through thin structures, where a phonon propagates through a solid, scattering diffusely off of any variety of boundaries, and reducing its effective thermal conductivity has prevailed.

Thermal transport, increasingly, has become a key factor in the design of electronic, photonic, and energy harvesting devices [17, 18]. With ever-more precise fabrication techniques, the scale of the devices used in these industries has continued to decrease. For example, in 2006, a 65 nm process for CMOS fabrication became standard [19]. Only six years later, in 2012, the scale of the standard prevailing process was down to 22 nm [20]. As these devices continue to shrink [21, 22], exponentially [23], they have placed different requirements on their thermal design. In electronic and photonic components, the Casimir picture of thermal conductivity reduction with reduced system size can severely degrade the performance of devices. For example, in the electronics industry, with the growth in the number of chip components per unit area, the thermal management problem grows as well. The would-be heat generation corresponding to using all of the components on a chip simultaneously at their maximum speeds could not be dissipated with today's thermal management designs and was the reason the semiconductor industry has migrated to multicore technology [24]. In thermoelectric energy harvesting, on the other hand, a reduced thermal conductivity improves the overall thermoelectric figure of merit of the device [25, 26]. Thus, the competing needs of various industries that employ nanoscale devices has motivated studies of thermal transport at these small length scales.

The research community has approached the study of nanoscale thermal transport with a combination of experimental and theoretical methods. In the experimental realm, helped by the improvements in fabrication techniques, the community has explored thermal transport through a variety of structures, including superlattices [27, 28], nanowires [29, 30], and nanoporous thin films [31]. To this point, experimental studies of these structures have largely pointed to the dominance of the Casimir picture, where interfaces between materials in the case of superlattices, or roughness at sample boundaries, in the case of nanowires and nanoporous films, cause phonons to scatter diffusively, reducing the overall thermal conductivity [17, 18]. More powerful hardware and computational algorithms have enabled a rapid increase in the capabilities and speeds of simulation methods such as first principles [32, 33], density functional theory (DFT) [34, 35], Green's functions [36, 37], molecular dynamics [38], monte carlo methods [39, 40], and Boltzmann transport equation calculations [41]. These computational methods have sometimes been used to support the work of experimentalists, and in other cases has elucidated new thermal transport regimes [42], inspiring work for future experimentalists.

In this thesis, we explore nanoscale thermal transport in superlattices (SLs) experimentally and computationally. We use optical methods to measure the different aspects of thermal transport, including their anisotropy, the coherent transport regime, and the breakdown of the coherent transport regime, through GaAs/AlAs SLs. These measurements are supported with first-principles and Green's functions calculations of thermal transport, which help shed light on the experimental results. The work herein helps offer insights into fundamental aspects of thermal transport. In addition, the novel approach to studying these structures, combining SLs with thin films, introduces a new experimental paradigm for future studies of thermal transport through nanostructures.

1.1 Nanoscale Heat Transport

Phonons, or quantized lattice vibrations, are the primary thermal energy carriers in semiconductors and dielectrics. They can be described with a language familiar from other fundamental energy carriers like photons and electrons, having an associated wavelength and velocity. These two properties can be readily derived from knowledge of a material's crystal structure using density functional theory [34], since the geometric configuration and the atomic makeup of the crystal structure can entirely define the nature of the possible quantized vibrations of the lattice. The crystal lattice alone assigns the allowable phonon modes, which are inherently discrete due to the discrete nature of the crystal lattice. In particular, the shortest phonon wavelength in a specific crystallographic direction equals twice the smallest lattice periodicity in that direction, while the longest vibrational wavelength extends throughout the whole material. Each possible phonon wave is assigned to a wavevector specifying the direction and wavelenegth of the wave. A map that describes the behavior of all of the phonons in the material by relating each phonon's wavevector to a frequency is called a dispersion relation. From the dispersion relation, it is possible to determine the relevant properties for thermal transport of the material, including the group velocities and populations of the phonons. The phonon lifetimes can be calculated once higher-order force constants, which can be determined from first principles calculations, are known [43, 44]. This information can yield the thermal conductivity, k, of a material through

$$k = \frac{1}{3} \int_0^{\omega} C_\omega v_\omega^2 \tau_\omega d\omega \tag{1.2}$$

where C_ω is the heat capacity, v_ω the group velocity, and τ_ω the lifetime of the particular phonon mode. In addition, the product of the group velocity and the lifetime yields the phonon's mean free path, or MFP Λ_ω, which describes the average distance a particular phonon mode, ω, travels between scattering events. This equality demonstrates that the bulk property we know as the thermal conductivity is in fact the integrated effect of transport contributed by every individual phonon mode.

The thermal conductivity, typically given in units of W/m-K, is a property of major interest for a vast array of applications because it describes the rate at which heat can travel through a material. Metals, whose main thermal energy carriers are electrons, tend to have thermal conductivities in the hundreds, while materials such as semiconductors and dielectrics, which are ubiquitous in applications ranging from electronics to energy harvesting and whose main thermal energy carriers are phonons, typically have conductivities in the tens to low hundreds. For example, at room temperature, bulk GaAs has a thermal conductivity of 45 W/m-K, while silicon has a bulk thermal conductivity of 142 W/m-K. However, the natural thermal transport properties of these materials are sometimes not aligned with their desired properties for specific applications.

Let us think about the example of thermoelectric energy harvesting. The principle of thermoelectric operation in the energy-harvesting regime is that a temperature difference leads to a diffusion of electrical energy carriers. A material's suitability for use in this application is judged with the thermoelectric figure of merit,

$$ZT = \frac{\sigma S^2 T}{k} \tag{1.3}$$

where σ is the electrical conductivity, S is the Seebeck coefficient, T is the temperature, and k is the thermal conductivity. Strictly speaking, the thermal conductivity here is the sum of the thermal conductivity due to both phonon thermal energy transport and electron thermal energy transport. Here we will focus on the phonon or lattice thermal conductivity, since in most thermoelectric materials, the contribution from electronic thermal transport is small. Equation (1.3) demonstrates that one strategy for increasing the thermoelectric figure of merit is to decrease the phonon thermal conductivity.

Looking back at Eq. (1.2), it is clear that to reduce the thermal conductivity it is necessary to reduce either the group velocity of the phonons or their lifetimes, assuming that the heat capacity remains unchanged. The group velocity, given by

$$v_g = \frac{d\omega}{dk} \tag{1.4}$$

is a property of the structure from which the dispersion relation arises. The lifetime can be manipulated with a much more brute force approach. Modifying the lifetimes, or the mean free paths (MFPs), requires manipulating the mechanisms of phonon scattering. This topic has been explored extensively over the last several decades with varying degrees of success. It is well-known, for example, that doping a material with a foreign element that disrupts order is a good method for reducing phonon thermal conductivity [14, 45]. In general, perturbations to the standard crystal lattice are an excellent way to reduce phonon thermal conductivity. Other perturbations include adding grain boundaries [26], removing or adding dopants to create a local lattice distortion [46, 47], and adding interfaces or boundaries [48]. In most of these cases, the reduced thermal conductivity can be attributed to the classical Casimir picture. In this picture, a lattice wave interacts with a scatterer, such as an interface, and in this interaction loses phase information. Due to this loss of phase, the phonon can be treated as a particle rather than a wave [15]. This Casimir picture has been invoked again and again to design and to model thermal conductivity reduction in crystals [17, 49]. However, the knowledge that heat phonons in crystals are in fact fundamentally waves, has compelled the research community to carry on in the hunt for manipulating wave effects in phonon heat conduction similarly to the way these wave effects are manipulated pervasively in the photonic and electronic industries.

1.2 Thermal Transport through Nanostructures

A number of structures have been constructed in an attempt to experimentally confirm the presence of wave effects in thermal transport. These structures include superlattices [27, 28], nanowires [29, 30], and nanoporous thin films [31]. In experimentally measuring the thermal conductivities of all of these structures, the reduction in thermal conductivity relative to the bulk parent material has been mainly attributed to the previously discussed Casimir picture. Several experiments, however, have resulted in observations that could not be fully explained with this classical scattering picture. These experiments, outlined in this section, have led to speculation that wave effects are, in one way or another, present in thermal transport through these structures. However, insufficient experimental evidence or a lack of rigorous and sophisticated modeling has thus far made proving the influence of these wave effects very difficult.

1.2.1 Superlattices

Superlattices (SLs), nanostructures comprising alternating layers of thin films, together referred to as a period, are a classical example of researchers trying to manipulate phonons in the wave regime [50, 51]. Although they were first proposed in 1970 by Leo Esaki and Raphael Tsu for use as an electron analog of a Fabry-Perot interferometer [52], heat transfer scientists seized the opportunity to use the 1-D system to better understand thermal transport [27, 28, 53, 54, 55, 56], believing it could also approximate an acoustic Bragg reflector.

In the analogy of the SL as an acoustic Bragg reflector with perfect interfaces and periodicity, as layers accumulate phonon stopbands, or regions of the dispersion relation where phonons cannot exist, will form (Fig. 1-1(A)). This is analogous to the photon stopbands in Bragg reflectors. In the solid-state picture, once several periods have been traversed, these stopbands correspond to bandgaps that open up in the dispersion relation at the Brillouin zone (BZ) edges (Fig. 1-1(B)). The dispersion relation itself is modified due to the quasicrystalline nature of the SL in the direction perpendicular to the interfaces, or the cross-plane direction.

As mentioned previously, the dispersion relation relates the frequency of the phonon modes to the discrete wavevectors, which are defined by the geometry of the crystal. The largest allowable wave vector is limited by the inverse of the length of the smallest repeated unit, or the primitive unit cell. In a homogeneous crystal, this length is the lattice constant. In a superlattice, the smallest primitive unit cell in the cross-plane direction is the thickness of the two layers that together form the period, so the unit cell is much larger than in a simple crystalline material. The largest allowable wavevector, therefore, is significantly smaller. This reduction in the size of the BZ is referred to as zone folding [57]. As long as phonons are not scattered internally in the layers of the SL or diffusively at the internal interfaces of the SL, this zone folding leads to two important effects that change thermal transport in the SL. One effect is that there are more phonon branches. This in itself opens more channels for phonon-phonon scattering [58]. These new phonon bands must have zero velocity at the zone edges. Thus, the phonon bands experience an overall flattening [58]. Recalling Eq. (1.4), we see that this means that there is a reduction in the phonon group velocities. According to Eq. (1.2), this effect would consequently reduce the thermal conductivity in SLs.

These results are the consequences of studying the superlattices theoretically as though they were new quasicrystalline materials. This harmonic picture and the resulting transmission peaks and valleys have been confirmed at very low temperatures, where anharmonic effects play a very small role [50, 59], with experiments that probed the transmission of specific phonon frequencies (Fig. 1-1(C)). But the challenge in seeing these effects in the thermal transport regime is that heat conduction is a broadband process, where all phonon modes participate. Additionally, for energy harvesting applications, greater interest lies in the behavior of nanostructures at higher temperatures.

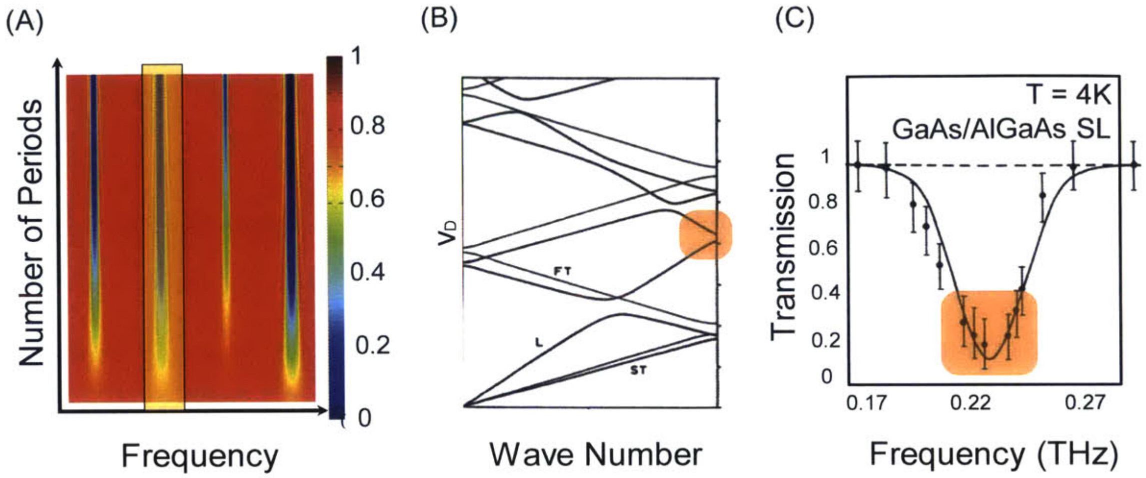

Figure 1-1: (A) Transmission stopbands result from coherent interference of propagating phonon modes; (B) in the solid-state picture, these stopbands correspond to bandgaps in the SL dispersion relation (figure reprinted from Tamura 1988); (C) these stopbands result in transmission dips that have been confirmed for individual frequencies at low temperatures (figure reprinted from Narayanamurti 1981).

Measurements of cross-plane thermal transport through superlattices have largely focused on observing the thermal conductivity trend as a function of temperature and superlattice period thickness [27, 28, 54, 60]. By and large, these studies have shown that the cross-plane thermal conductivity of SLs increases with increasing period thickness (Fig. 1-2). In these studies, the reduced thermal conductivity was attributed to the Casimir picture. Specifically, the samples were fabricated to be thermally thick for the experiments that were performed on them. In that case, when the same thickness was probed in superlattices with different period thicknesses, those with thinner periods included more interfaces. The data have been interpreted as demonstrating that phonons traverse the internal layers of the superlattice ballistically, but scatter diffusively at the internal interfaces. These interfaces, acting like classical scatterers, increased the overall thermal resistances of the SLs, decreasing their apparent thermal conductivities.

This invocation of the Casimir picture has been confirmed by the lack of agreement between the experimental results and a variety of theoretical studies that have actually shown that the thermal conductivity decreases very slightly or remains nearly unchanged with increasing period thickness when roughness at the interfaces is not included. Lattice-dynamic simulations, which can be used to calculate these bulk thermal properties by integrating over all frequencies and include only these coherent phonon transport effects, show that with increasing period thickness, denoted here by '*d*,' the thermal conductivity stays nearly constant (Fig. 1-2(A)) [58, 61, 62, 63]. In Boltzmann transport equation (BTE)-based models, although both specular and diffuse reflections at interfaces were considered, the phase information that would be required for the buildup of phonon stopbands was not considered [55]. More recently, first-principles simulations have similarly shown a nearly constant thermal conductivity with increasing period thickness [64]. Even in the case of the simulations, however, when some interface roughness and the Casimir picture are added to the model, the resulting thermal conductivity can frequently match the experimental trends fairly well [55].

Finally, it should be noted that we have primarily discussed cross-plane thermal transport in SLs so far, but transport parallel to the interfaces, or in-plane transport, is also of interest for electronic, photonic, and thermoelectric applications since anisotropic transport can have a big effect on thermal management considerations. Additionally, the same factors (interface scattering, reduced group velocities) that change the thermal transport in the cross-plane direction are also expected to have an effect in the in-plane direction [65, 66].

The first thermal conductivity measurements in SLs were performed with AC-calorimetry in the in-plane direction of GaAs/AlAs SLs [67]. AC-calorimetric studies, however, rely on freestanding SL films, which are difficult to fabricate. Other experimental methods such as the 3ω method, the two-wire 3ω method, and time-domain thermoreflectance are much more sensitive to cross-plane thermal transport [68]. The measurements that do exist have also largely been explained with the Casimir picture [53].

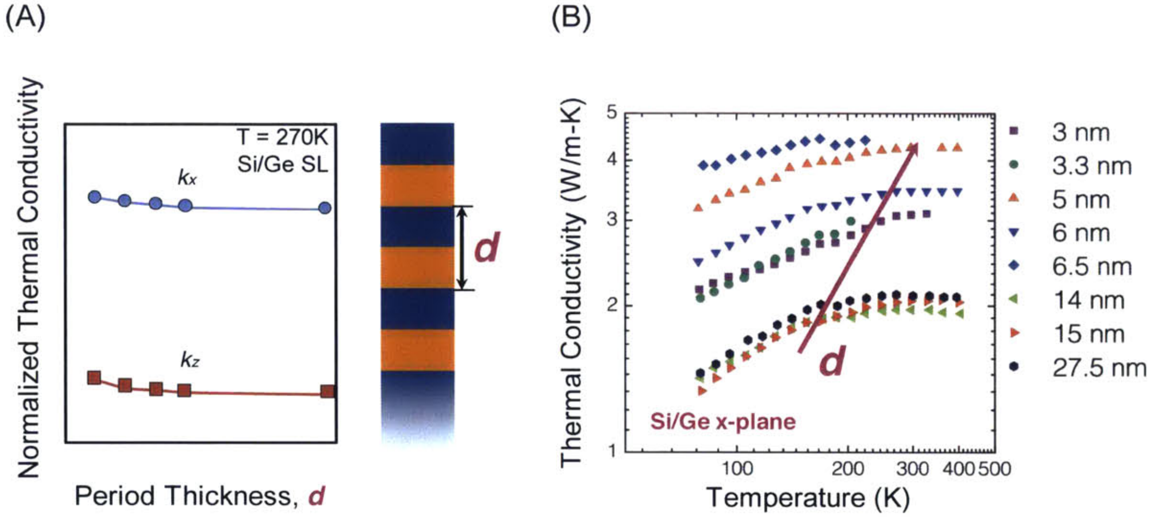

Figure 1-2: (A) Lattice dynamics prediction of SL thermal conductivity as a function of period thickness; (B) experimentally determined trend of thermal conductivity with period thickness (figure reprinted from Lee 1997.)

1.2.2 Nanowires

Nanowires have proven to be an excellent tool for examining the effects of boundary scattering on thermal transport. A reduced thermal conductivity compared to the bulk parent materials has been demonstrated in a range of nanowire and nanowire-like structures, including Si [30, 69, 70, 71], Bi_2Te_3 [72], SiGe [73], and Bi [74] nanowires. In most of these cases, the thermal conductivity decreased monotonically with a reduction in the nanowire diameter. In cases where there was the possible presence of defects within the nanowires, the Casimir picture explained well the reduced thermal conductivity, when scattering from the impurities and defects was included. In one case [71], where the purity of the silicon nanowire was high and the roughness of the surface was carefully measured and catalogued, the greater thermal conductivity reduction with decreasing diameter that was experimentally observed, compared to that predicted by including only the Casimir picture, was attributed to the possible presence of wave effects since the Casimir picture was insufficient in explaining the full reduction effect.

However, insufficient modeling is available to verify these wave effects. Some models which artificially reduced the phonon MFPs and ascribed different specularity parameters, or quantizations of the scale of disorder at the nanowire boundaries, for different groups of phonons have been unable to replicate the exact scale of the thermal conductivity reduction. Instead, further scattering in the body of the nanowires due to the presence of impurities or an alloying effect must be invoked to match the experimental data [75].

In one study, the directional dependence of heat flow through a boron nitride nanotube (BNNT) that was asymmetrically loaded with $C_9H_{16}Pt$ was observed [76]. The group employed a commonly-used platform for studying thermal transport through individual nanowires [29] and found that the thermal conductance was asymmetric through these wires. This rectification effect was attributed to the presence of solitons, or non-dispersive lattice waves, in thermal transport. While this is yet another example of the search for wave effects in thermal transport, it has yet to be verified with simulations or analytical proofs.

1.2.3 Nanoporous thin films

Finally, films or ribbons with periodic arrays of holes have recently become a popular structure for trying to understand nanoscale thermal transport [31], motivated by a modified dispersion relation expected with the new quasicrystalline structure. Experiments on nanoporous silicon films have shown thermal conductivities approaching the thermal conductivity of amorphous silicon [31]. These structures provide a major advantage over amorphous silicon in energy harvesting applications because, while they appear to be excellent at scattering phonons and thus reducing heat transport, they largely maintain their electrical properties [77]. A number of effects are in play in reducing the thermal conductivity of these nanoporous silicon structures compared to bulk Si. One such effect is that the material system no longer consists only of silicon, but also of the vacuum in the periodic pores. This effect can be accounted for with the effective medium theory, where the thermal properties are determined with a weighted average of the thermal properties of the two components. In addition, the boundaries at the silicon-air interface are imperfect, and the diffuse scattering by them can have a large effect in reducing the phonon thermal conductivity [78]. Finally, the larger scale crystallinity imposed by the periodic holes leads to a modified dispersion relation with reduced group velocities for reasons analogous to those in superlattices [79, 80]. This was the explanation invoked by [31] because the thermal conductivity was lower than that predicted by classical scattering off the hole boundaries. However, recent Monte Carlo solutions of the Boltzmann Transport Equation were able to replicate the results of the experiments and found that the lowered thermal conductivity was explained by incoherent boundary scattering from the holes [81].

1.3 Phonon Wave Effects in Superlattices, Revisited

While the previous demonstrations of potential wave effects in nanostructures have been encouraging, they have remained somewhat unproven because modeling such complicated structures has been difficult. In order to detect wave effects, we took a different approach, building upon a fundamental understanding of phonon transport through materials and at interfaces.

In the diffusive picture of thermal conduction, carriers go on a random walk from hot side to cold side, undergoing many scattering events and losing any of their phase information (Fig. 1-3(A)). In the ballistic regime, phonons traverse the region without scattering at all until they reach a boundary or an interface. As the Casimir picture suggests, at the boundary, they scatter completely diffusely and lose any of their coherence, i.e. phase information (Fig. 1-3(B)).

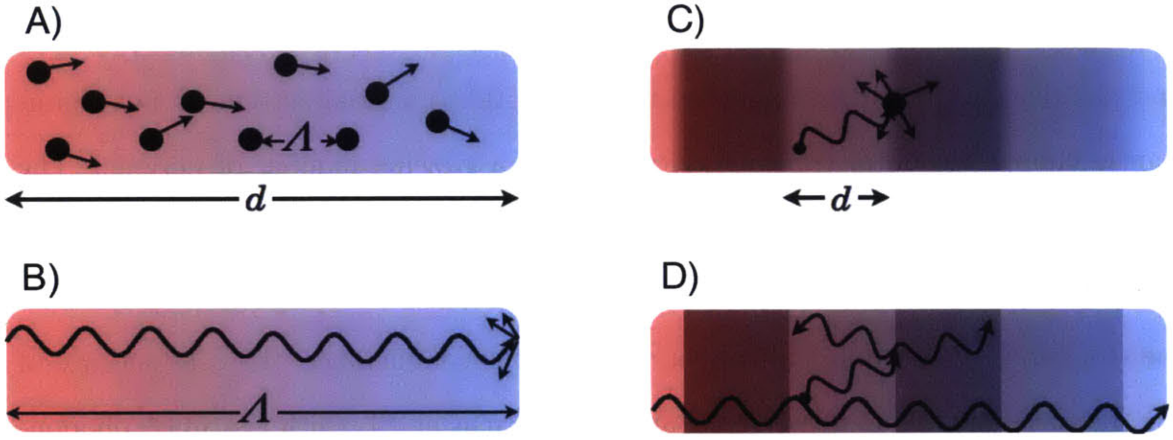

Figure 1-3: Schematic depiction of phonon transport in transport through (A) a bulk material whose thickness is much greater than the phonon mean free path, Λ; (B) a single-component material whose thickness is less than the phonon mean free path; (C) a multilayer system with diffuse boundary scattering at the interfaces, and (D) a multilayer system with specular boundary scattering at the interfaces.

In a multilayer where each internal layer is thinner than the phonon mean free path, the phonon can traverse the layer ballistically, without experiencing any internal scattering. At an interface, the phonon can scatter diffusively, leading it to lose its phase information and any coherence (Fig. 1-3(C)). In this case, the multilayer behaves like a composite material, where each interface behaves as a diffuse scatterer with a nearly fixed resistance [1]. Adding multiple such layers together is then the equivalent of adding resistors in series. Alternatively, the phonon can reach the interface, and be reflected or transmitted specularly (Fig. 1-3(D)). In this case, multiple reflections and transmissions will lead to the coherent superposition of the phonon Bloch waves and the nanostructure will behave like a homogeneous material with its own unique dispersion relation.

In the fully coherent regime, the reflected and transmitted phonon waves at the interfaces between layers interfere with each other, leading to phonon frequency stopbands in which destructive interference in the structure completely cancels phonon waves in the material. It turns out that, when integrated over all phonon frequencies and polarizations, such stopbands in the GaAs-AlAs material system do not significantly change the total transmissivity through a growing number of periods. The Landauer formalism, which is used in the coherent limit to determine the thermal properties of the SL, relates conductance to the phonon transmissivity [82]. Because the stopbands play a minimal role in changing the conductance, the conductance of the SL turns out to be nearly constant with increasing SL thickness until phonon-phonon scattering becomes important. The thermal conductivity is related proportionally to both the conductance and the thickness of the SL. Since the conductance with varying period numbers is nearly constant, it is this linear growth with SL thickness that dominates the thermal conductivity trend (Fig. 1-4(A)).

We expect a different behavior if incoherent transport dominates (Fig. 1-4(B)). In a coarse-grained picture of the SL, we expect that each additional layer and the included interfaces are equivalent thermal resistors. These resistors act in series, so the total conductance decreases with the number of periods. Since both the resistance

---

[1] A previous study has demonstrated, through the numerical evaluation of the Boltzmann transport equation, that with a changing period thickness, the non equilibrium phonon distribution on either side of the interfaces changes as well. This result indicates that the thermal boundary resistance is not an intrinsic property of the SLs, but can also be thickness dependent [55].

and the thickness grow linearly with thickness, these effects cancel, and the thermal conductivity is constant and independent of the SL geometry (Fig. 1-4(B)). Thus, examining SL behavior at the scale of thin films, i.e. observing the SL thermal conductivity dependence on the total thickness of the SL, is a promising avenue for detecting coherent wave effects.

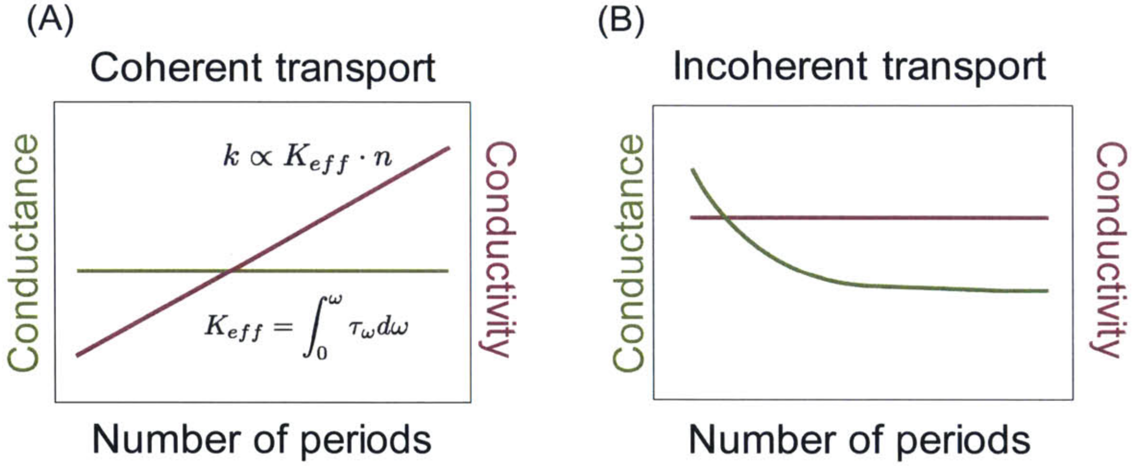

Figure 1-4: Expected thermal transport properties in the case of (A) coherent and (B) incoherent phonon transport.

1.4 Time-Domain Thermoreflectance

The need for understanding thermal energy transport at the nanoscale has led to a number of experimental advances that allow for the probing of thermal energy transport at these small scales without making contact with the sample. Time-domain thermoreflectance, or optical pump-and-probe [83], studies have become one of the dominant of these non-contact thermal transport measurement techniques. Briefly, in TDTR, a strong laser pulse impinges on a metal optothermal transducer on the sample, exciting electrons in the metal which quickly thermalize, sending a heat pulse propagating through the length of the sample. As the heat dissipates away from the top metal surface of the sample, its reflectivity changes, and this changing reflectivity is measured and mapped in time by a time-delayed probe laser pulse. This changing reflectivity can be directly related to the changing sample surface temperature. The resulting temperature decay curve is fit with a least-squares minimization algorithm to a multi-layer, multi-dimensional solution of Fourier's law. The unknown variables, usually the thermal conductivity of the sample and the interface conductance between the sample and the optothermal transducer, for solving this equation are thus determined [68, 84, 85].

In our particular measurement system, shown in Fig. 1-5, a tunable pulsed Ti:sapphire laser emits a collimated 80 MHz pulse train with 200 fs pulses at a center wavelength of 800 nm and a time-averaged power of approximately 1 W. The red light is sent through an optical isolator that prevents potentially destabilizing back-reflections into the laser. The light is then split with an adjustable waveplate and a polarizing beam-splitter into two arms, a pump arm and a probe arm. The pump arm, comprising about 95% of the initial output energy from the laser, passes through an electro-optical modulator (EOM) which operates in the low MHz regime. The light is modulated by the EOM to enable lock-in detection. The light then passes through a BBO frequency-doubling crystal, where the red light is converted into blue light with a frequency of 400 nm. The blue light passes through an objective, which focuses it onto the sample with an adjustable spot size ranging from approximately 10 to 100 μm. In this thesis, the pump spot size was held constant at 60 μm, yielding an intensity on the sample of 7x10^7 W/ cm2. The net temperature rise at the surface of the sample resulting from the pump pulse is on the order of several degrees K [54].

After splitting off from the main pulse train, the collimated probe arm is directed through an expander which quadruples its radius and then a mechanical delay stage which can add up to 2 m to its path, or delay the arrival of a pulse by up to 6.5 ns compared to the undelayed pump pulse. The probe beam then goes through a telescope where the spot is recompressed. Finally, the probe arm passes through the same objective that focuses the spot on the sample to a radius of 10 μm. Thus, after a pump pulse impinges on the surface of the sample, the reflectivity is measured at various time-delays between 0 and 6 ns by the much weaker probe pulse. The power of the reflected probe pulse is measured with a Si diode amplified detector and recorded. A schematic of the TDTR experimental setup used in this thesis along with a sample dataset is shown in Fig. 1-5.

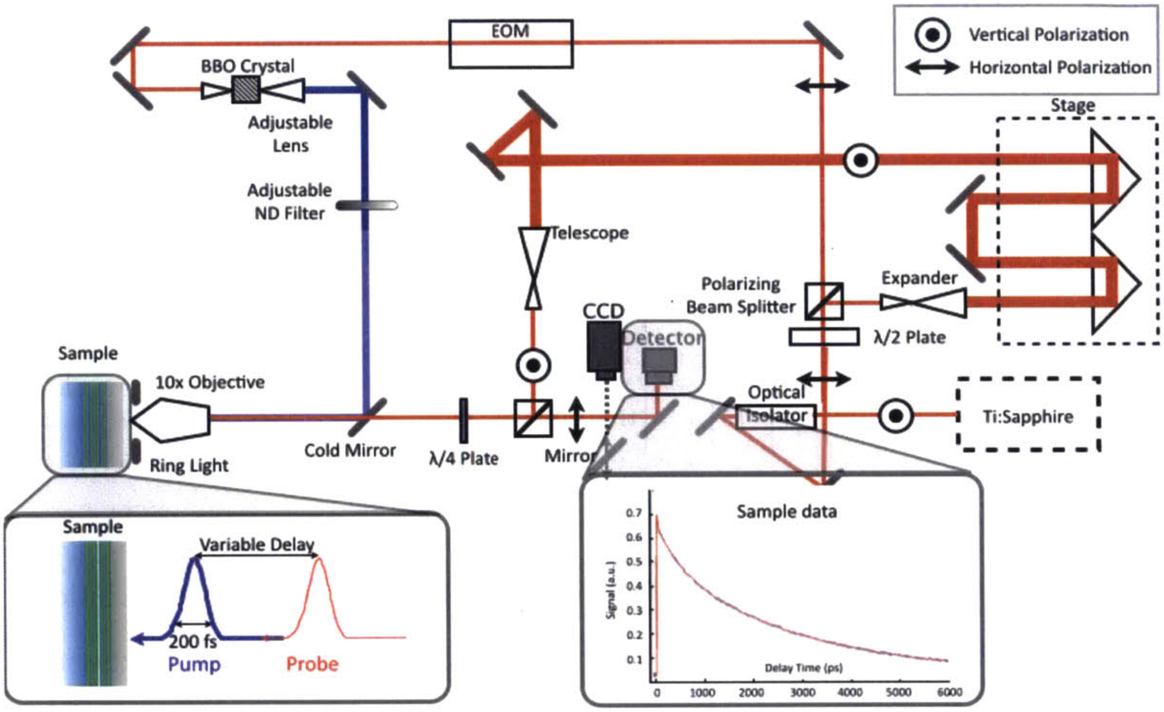

Figure 1-5: Schematic diagram of the time domain thermoreflectance experiment used in this thesis.

Thermal transport through a single layer is modeled in the frequency domain as

$$\begin{bmatrix} T_b \\ f_b \end{bmatrix} = \begin{bmatrix} cosh(qd) & \frac{-1}{\sigma_z q} sinh(qd) \\ -\sigma_z q sinh(qd) & cosh(qd) \end{bmatrix} \tag{1.5}$$

where T_b and T_t are the temperature of the bottom of the layer and the top of the layer, respectively, f_b and f_t are the heat flux through the bottom and the top of the layer, respectively, d is the layer thickness, σ_z is the through-plane thermal conductivity, and $q = \sqrt{i\omega/\alpha}$, where α is the thermal diffusivity [86]. When multiple layers are involved, the front-side and back-side conditions are met by multiplying matrices for every layer together. One additional wrinkle is presented by the interfaces between layers, which can cause a thermal resistance that is conditional on the different structures of the materials or the deposition quality. The interface resistance causes a temperature drop from the bottom side of one layer, T_{b1}, to the top side of another layer, T_{t2}, and therefore a heat flux, f, determined by

$$f = G(T_{b1} - T_{t2}) \tag{1.6}$$

where G is the interface conductance. The matrix element for the interface is thus

$$\begin{bmatrix} T_{t2} \\ f \end{bmatrix} = \begin{bmatrix} 1 & G^{-1} \\ 0 & 1 \end{bmatrix} \begin{bmatrix} T_{b1} \\ f \end{bmatrix} \tag{1.7}$$

The product of the matrices associated with the different layers yields the relationship between the transient temperature of the surface of the metal and the thermal properties of the constituent layers of the sample. This surface temperature is then matched to a heat diffusion equation model and the properties that best fit the model are determined. The necessary information for each layer is thus the heat capacity, the thickness, the through-plane thermal conductivity, and the anisotropy. Because the laser spot size and thus the heated area of the sample are usually much larger than the total thermal penetration depth, the anisotropy in the thermal conductivity of the samples is usually unimportant in the data fitting. The heat capacity values for all the experiments performed in this thesis were taken from the literature and the thicknesses were known from the growth parameters for the samples used.

1.5 Organization of this Thesis

In this thesis, we explore the wave effects in heat conduction by measuring thermal transport through superlattices. In Chapter 2, we measure the thermal conductivities of GaAs/AlAs SLs with two different period thicknesses: 2 nm x 2 nm, for a period of 4 nm and 8 nm x 8 nm, for a period of 16 nm. The thermal conductivities are measured in both the cross-plane direction, with TDTR as described above, and the in-plane direction with transient thermal grating, or TTG. Using these two optical methods in tandem yields some of the first results on the anisotropy of the same SL samples. The anisotropies of the SLs lend insight into the scattering modes of the superlattices. The measurements are complimented by first-principles modeling. The good match between the modeling and the results of the experiments gives us confidence in the modeling methods which are used in later chapters to help understand experimental results on coherent phonon transport through SLs.

In Chapter 3, we delve deeper into the scattering modes with a new paradigm for measuring thermal transport through SLs. As mentioned previously, most experiments conducted on SLs have measured the heat transport through thermally thick SLs with varying period thicknesses. In this and the subsequent chapter, we have measured SLs with constant period thicknesses, but different numbers of periods. This new paradigm has given us access to entirely new regimes of phonon scattering. Specifically, in Chapter 3 we experimentally observe for the first time and theoretically confirm coherent phonon heat conduction, a regime that had remained elusive in experiments on such nanostructures. The experimental results are further elucidated with first-principles and Green's functions simulations.

Building upon the success of this new experimental model, in Chapter 4 we measure GaAs/AlAs superlattices with and without additional scatterers in the form of ErAs nanodots at the interfaces. Through this experiment, we not only confirm the coherent phonon heat conduction observed in Chapter 3, but we also detect the phenomenon of phonon localization, which was also previously unobserved in thermal transport. Finally, in Chapter 5 we discuss the possible future research directions that the results presented in this thesis suggest.

Chapter 2

Anisotropy of the Thermal Conductivity in GaAs/AlAs superlattices

Most material reprinted with permission from M. N. Luckyanova, J. A. Johnson, A. A. Maznev, J. Garg, A. Jandl, M. T. Bulsara, E. A. Fitzgerald, K. A. Nelson, and G. Chen "Anisotropy of the Thermal Conductivity in GaAs/AlAs Superlattices," *Nano Lett.* **13** (9), 3973-3977 (2013). Copyright 2013, American Chemical Society.

In this chapter, we address the problem of measuring the anisotropic thermal conductivity of thermally thick superlattices (SLs). As mentioned in Chapter 1, this problem has plagued experimentalists for several decades and the few experimental results of in-plane thermal conductivity have primarily come from the AC-calorimetric or 3ω methods. However, performing cross-plane and in-plane measurements on the same sample is difficult, and very little data on the anisotropy of the thermal conductivity in SLs exists. Results of the measurement are important for understanding superlattice thermal transport and for validating the computational models of coherent phonon scattering in superlattices as well as interface scattering.

2.1 Introduction

The thermal properties of superlattices are of great interest in a range of fields. Due to their decreased thermal conductivities, SLs are an important fundamental learning tool for developing better thermoelectric energy conversion materials [87, 88]. In optoelectronics, SLs often serve as the gain media or the mirrors in solid-state semiconductor lasers, even though their low aggregate thermal conductivities often lead device temperatures to rise, degrading performance [89]. SLs are expected to have anisotropic thermal properties, resulting from both the modified phonon dispersion [61, 65] and increased diffuse scattering of phonons at the interfaces [55, 66]. So far, only a few studies have been conducted on the anisotropy of Si/Ge SLs by using the 3ω method and varying the linewidths of the heaters placed on Si/Ge SLs [90, 91, 92, 93].

Measuring the thermal conductivity anisotropy of SLs has proven challenging because frequently used techniques such as the 3ω method [94] and optical pump-probe [84] are more sensitive to cross-plane thermal transport [68]. Measurements of in-plane thermal properties using AC-calorimetry rely on freestanding films [67, 95]. The 2-wire 3ω method characterizes thermal conductivity anisotropy of SLs by using two heaters of different widths, with one being much wider than the thin film thickness so that its temperature rise is independent of the in-plane thermal conductivity of the film. The other heater has a width smaller than or comparable to the film thickness, such that its temperature rise depends on heat spreading laterally inside the film, making this measurement sensitive to the in-plane thermal conductivity. However, due to the dominance of the cross-plane thermal conductivity in determining both heaters' temperature rise, the sensitivity to the in-plane thermal conductivity is limited and depends on the film thickness as well as the thermal conductivity anisotropy

[92].

Extensive theoretical and modeling studies [41, 96] have been carried out on heat conduction mechanisms in SLs using lattice dynamics [58, 61] and molecular dynamics simulations [97]. Continued experimental and theoretical studies deepen our understanding of the heat conduction mechanisms in SLs, which serve as excellent platforms to explore and engineer nanoscale phonon heat conduction [98]. Experimental tools capable of measuring the anisotropic thermal conductivity of SLs, and thin films in general, are needed. In this chapter, we combine the transient thermal grating (TTG) and time-domain thermoreflectance (TDTR) techniques to characterize anisotropic thermal conductivity. Using this combination, we report the anisotropic thermal conductivity of GaAs/AlAs SLs and compare the experimental results with first-principles calculations and previous measurements of thermal conductivity anisotropy in Si/Ge SLs.

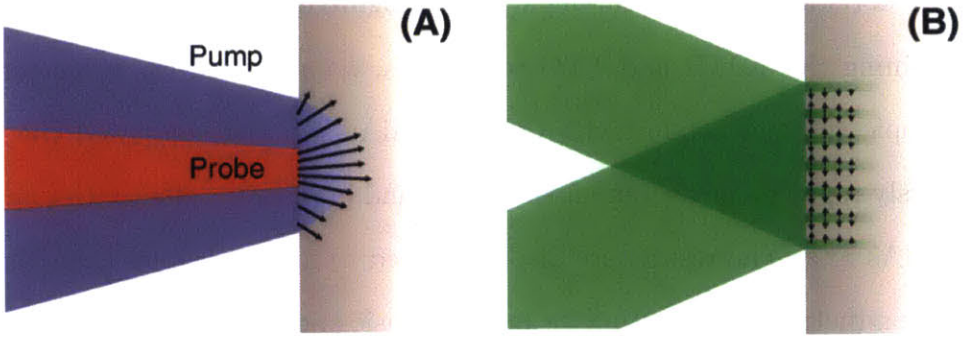

Figure 2-1: Schematic diagram of the laser excitation and subsequent heat diffusion pathways due to **(A)** the time-domain thermoreflectance (TDTR) setup and **(B)** the transient ther-mal grating (TTG) setup.

2.2 Experimental Implementation

We used two non-invasive optical techniques in tandem to measure the anisotropic thermal properties of two GaAs/AlAs SLs grown with metal organic chemical vapor deposition (MOCVD). The TDTR technique [68, 84, 99] was used to measure the cross-plane thermal conductivities and TTG [100, 101, 102, 103, 104, 105, 106] was used to measure the in-plane thermal diffusivities. These two techniques have not been combined before to characterize the anisotropy of thermal transport in thin films and SLs. Both techniques use lasers to induce a temperature rise at the sample surface and to monitor the temperature decay via heat conduction. The main difference between the two techniques lies in the spatial distribution of the excitation laser light at the sample surface, as illustrated in Figs. 2-1(A) and (B). In TDTR (Fig. 2-1(A)), we used a large (60 μm) laser spot; hence on short time scales the heat transfer occurs primarily in the cross-plane direction. In TTG (Fig. 2-1(B)), two interfering beams created a sinusoidal intensity pattern with a small period (on the order of a few microns). The heat transport in TTG occurs in both the in-plane and the cross-plane directions; however, as will be explained below, the temporal signature of the thermal grating decay is only sensitive to the in-plane thermal conductivity. This unique characteristic of the measurement was recognized only recently [103].

By combining the TDTR and TTG techniques, we measured the room temperature anisotropic thermal conductivity of GaAs/AlAs SLs and compared the results with previously reported measurements of cross- and in-plane conductivities on different GaAs/AlAs SLs. The results are also compared to first-principles calculations of SL thermal conductivity, accounting for both intrinsic and extrinsic phonon scattering channels, and the results are contrasted with experimental data on Si/Ge superlattices, which have a larger acoustic mismatch.

2.2.1 Sample preparation

Two 3.5 μm thick GaAs/AlAs SLs, an 8 nm x 8 nm (with a total period of 16 nm) SL and a 2 nm x 2 nm (with a total period of 4 nm) SL, were epitaxially grown by MOCVD on the [100] direction of a GaAs wafer with a 500 nm GaAs buffer. X-ray diffraction measurements performed on the samples confirmed both the planarity and the period thicknesses of 4 nm and 16 nm for the two SL samples. For the TDTR measurements, a 90 nm Al optical-thermal transducer layer was deposited on the SL sample with e-beam evaporation [54].

2.2.2 Time-domain thermoreflectance

In the TDTR pump-probe measurements, a pump laser pulse (pulse duration 200 fs, wavelength 400 nm, spot size 60 μm, repetition rate 80 MHz, modulation frequency 3-12 MHz) impinged upon the sample, generating hot electrons in the metal transducer layer. The hot electrons quickly thermalized through electron-phonon interactions. Since the pump spot size is much larger than the thermal penetration depth, the resulting heat input propagated from the metal layer into the SL primarily in a direction perpendicular to the SL interfaces. A time-delayed probe pulse (pulse duration 200 fs, wavelength 800 nm, spot size 10 μm, repetition rate 80 MHz) measured the transient reflectivity of the surface of the metal transducer. This surface reflectivity is directly related to the surface temperature via the thermoreflectance coefficient. The resulting cooling curve was fit to a three-layer thermal diffusion model of the cooling of the sample. The layer structure consists of a thin metallic film, a finite thermal interface conductance between the metal transducer and the SL, and an anisotropic SL layer with an adiabatic back boundary. Fourier's law dictates the flow of heat within the metal transducer film and within the SL and is given by

$$C_i \frac{\partial T_i(z,t)}{\partial t} = k_i \frac{\partial^2 T_i(z,t)}{\partial z^2} \tag{2.1}$$

where C_i is the heat capacity and k_i is the cross-plane thermal conductivity of the layer i. There is a finite thermal resistance between the Al optical-thermal transducer layer and the SL due to the Kapitza resistance, G, given by

$$C_{Al}d\frac{\partial T_{Al}(z=d,t)}{\partial t} = -G(T_{Al}(z=d,t)) - T_s(z=0,t)) \tag{2.2}$$

where C_{Al} is the heat capacity and d the thickness of the Al, T_f is the temperature of the film and T_s is the temperature of the SL. A multi-parameter optimization was used to deduce the two unknown quantities: the thermal conductivity of the SL and the thermal interface conductance between the Al and the SL. The details of the experimental technique and data analysis have been discussed elsewhere [27, 68, 99].

2.2.3 Transient thermal grating

The in-plane thermal conductivity was measured using a transient thermal grating (TTG) technique by Jeremy Johnson of Prof. Keith Nelson's group at MIT. In this technique, two excitation pulses (pulse duration 60 ps, wavelength 515 nm, spot size 600 μm, repetition rate 1 kHz) interfered with each other on the surface of the sample to create a sinusoidal intensity profile with spacing L on the order of several microns (Fig. 2-2). Absorption led to a spatially periodic heating, and a spatially periodic variation in the sample optical properties, forming a transient diffraction grating that encoded the material thermal response. A diffracted quasi-cw probe beam (wavelength 532 nm, spot size 300 μm), superposed with a reference beam in a heterodyne detection scheme [103, 104, 105], was monitored to measure the temperature dynamics. Approximately 300 measurements were conducted per second so that each resulting signal decay (Fig. 2-3(B)) represents the average of 10,000 traces.

In general, the diffracted beam intensity was sensitive to both surface displacement and temperature "gratings" whose distinct time dependences can complicate the analysis of the diffracted signal decay measured in the reflection geometry. Heterodyne phase control was used to eliminate the surface displacement component which

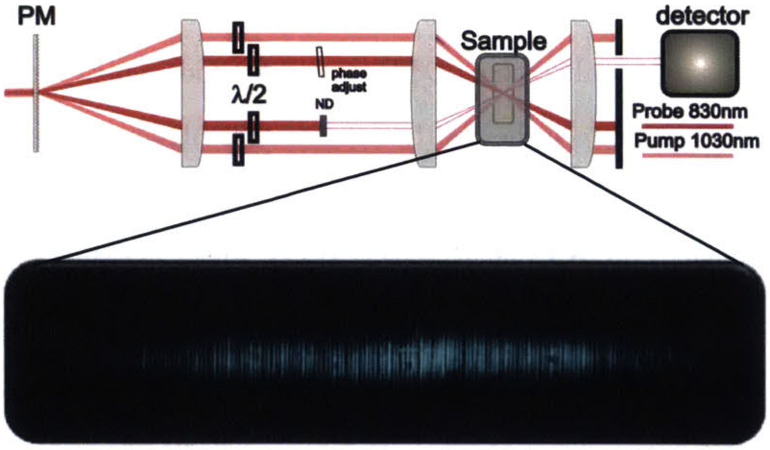

Figure 2-2: Schematic diagram of the TTG optical pump-and-probe experimental setup.

only contributes to the signal through its effect on the optical phase [103]. Thus the signal decay that we measured (Fig. 2-3(B)) tracked the dynamics of the amplitude of the spatially sinusoidal temperature grating at the sample's front surface.

The solution of the thermal diffusion equation [96] yields the following equation for the dynamics of the thermal grating decay at the surface $z = 0$:

$$T(z = 0, x, t) = T-)e^{\alpha_z \zeta^2 t} efrc(\zeta\sqrt{\alpha_z t}) cos(qx) e^{-\alpha_x q^2 t} \tag{2.3}$$

where ζ is the optical absorption coefficient, $q = \sqrt{2\pi/L}$ is the wave vector magnitude of the thermal grating, α_z and α_x are the cross-plane and in-plane thermal diffusivity values, respectively, and erfc is the complementary error function. The decay is influenced by both cross- and in-plane diffusivities; however, the former only affects the initial shape of the decay; at long times $t > \alpha_z^{-1}\zeta^{-2}$, Eq. (2.3) takes the asymptotic form

$$T(z = 0, x, t) = \frac{T_0}{\pi^{1/2}\zeta}(\alpha_z t)^{-1/2} cos(qx) e^{-\alpha_x q^2 t} \tag{2.4}$$

The temporal profile of the signal decay is completely determined by α_x, while

α_z only affects the amplitude factor. Thus the TTG method is selectively sensitive to the in-plane diffusivity unlike the TDTR or 3ω methods which, depending on the configuration, are sensitive to either both in- and cross-plane thermal conductivities or primarily to the cross-plane conductivity. This unique characteristic makes the TTG technique ideally suited to characterize the in-plane thermal conductivities of superlattices. In our SL samples, we estimate the absorption coefficient at the excitation wavelength to be 4×10^4 cm^{-1}. Consequently, the cross-plane diffusivity influences the decay dynamics only at short times, $t \leq 10$ ns. Indeed, Fig. 2-3(B) shows that the measured decay curves can be accurately fit with Eq. (2.4) for $t > 10$ ns.

Equations (2.3) and (2.4) are obtained for a uniform anisotropic half-space and do not account for the presence of the substrate. This is justified as long as the thermal grating decays before it can extend deeply enough to reach the substrate. The thermal penetration depth into the substrate is given by $h \sim 2(\alpha_z t)^{1/2}$. Considering that the time window used for the data analysis was 10-150 ns, let us take $t = 150$ ns; with the highest value of α_z measured using the TDTR method we get $h \sim 1.8\mu m$, significantly shorter than the SL thickness of 3.5 μm. For a longer TTG period, the time window of the experiment would be longer in order to allow in-plane heat transport from the grating peak to null, and thus the thermal penetration depth would increase. Since the GaAs substrate has a much higher diffusivity than the SL, we would expect the apparent diffusivity to go up with a longer grating period if the substrate effect becomes significant. However, for the TTG period range used in our measurements, 2.5-5 μm, the diffusivity was nearly constant, as shown in the inset in Fig. 2-3(B), giving us another indication that the substrate effect is negligible.

In the TTG method, in contrast with the TDTR method, we do not use a metal coating. This is an important difference that deserves a brief discussion. Measuring an uncoated sample entails a number of advantages: no sample preparation is required and the measurements are affected neither by the metal film thickness nor by the thermal boundary resistance at the metal-semiconductor interface [84]. Thus, there is no need to employ multi-parameter fitting. In fact, in the model we use to fit the data, given by Eq. (2.4), the only variable parameter is the parameter of interest, the in-plane thermal diffusivity. On the other hand, photothermal measurements on uncoated semiconductors are often complicated by the presence of photoexcited carriers [107].

Indeed, laser excitation creates both a temperature grating and a concentration grating of the excited carriers with the latter also influencing the refractive index and contributing to diffraction of the probe beam. However, the ambipolar diffusion coefficient of photoexcited carriers in both bulk GaAs [108] and GaAs quantum wells [109] exceeds 10 cm^2/s, whereas the thermal diffusivity measured on our samples is well below 0.1 cm^2/s. Consequently, the carrier grating should decay much faster than the thermal grating. Indeed, we do observe a small initial spike of duration 0.5 ns limited by the resolution of the detection electronics, which may be caused by the photoexcited carriers. On the longer time scale of interest, the carrier contribution should be entirely negligible, which is confirmed by the fact that the thermal model alone generally fits the data very well.

The above discussion makes it clear that the combination of the TDTR and TTG methods is a powerful new solution to the challenge of determining the anisotropic thermal conductivity of thin films and is ideally suited for studying the physics of phonon heat conduction in SLs. Figure 2-3(A) shows raw data and the corresponding fitting curves from the TDTR experiment for the SLs we studied. Figure 2-3(B) shows the data and fitting for the TTG experiment at four different grating periods. The solid lines are measured data and the dashed lines are fittings to the data with Eq. (2.4).

2.3 Results

The experimental in-plane and cross-plane thermal conductivities as well as the resulting anisotropies are given in Table 1. The anisotropy is defined as the in-plane thermal conductivity divided by the cross-plane thermal conductivity. Thermal conductivity, k, values in the table are obtained from experimentally measured thermal diffusivities via $k = \rho c_p$, where c_p is the average of the specific heats of GaAs and AlAs and ρ is the average of their densities [110]. For the TDTR experiments, each SL was measured at five different randomly selected locations under four different pump modulation frequencies. No systematic frequency dependence was found. Thus, the thermal conductivities given represent the averages of 20 measurements and the standard deviation of these measurements. The error given for the TTG measurements is the standard deviation in the five grating spacing measurements shown in the inset of Fig. 2-3(B). The thermal conductivities are lower than the corresponding bulk values. The table also shows the values for in- and cross-plane thermal conductivities in 2 nm x 2 nm Si/Ge symmetrically strained SLs as well as the resulting anisotropy, obtained using the 3ω method with two different heater widths [91]. The results indicate that the anisotropy is significantly higher in the Si/Ge SLs due to the larger mass difference and the corresponding mismatch in the phonon properties between the Si and Ge layers, compared to that between the GaAs and AlAs layers.

A comparison of our results from these experiments with previously reported measurements for GaAs/AlAs SL thermal conductivities is shown in Fig. 2-4 [53, 54, 67]. The new data fit in well with the general trend of increasing thermal conductivities with increasing GaAs/AlAs SL period thickness. Variations among data reported by different authors are expected because phonon mean free paths (MFPs) in SLs are strongly influenced by defect scattering and interface roughness [55, 66] which could vary depending on the fabrication process. Since previous in-plane and cross-plane data were obtained on different samples, they do not provide reliable information

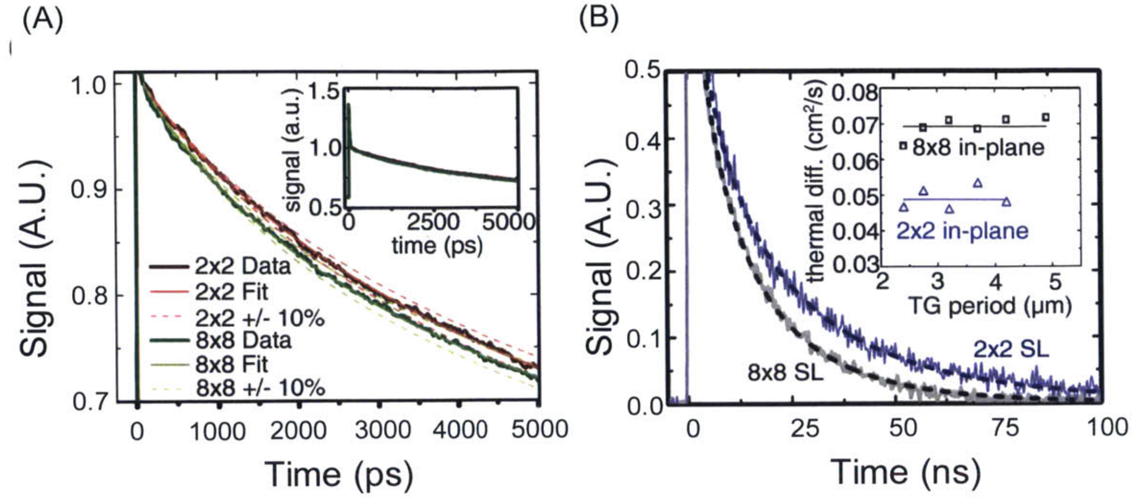

Figure 2-3: (A) TDTR and (B) TTG data and fits for the two SLs. The inset in (B) shows the thermal diffusivities of the two SLs at varying TTG periods.

about the thermal conductivity anisotropy of thermal conductivity in a given material system.

2.4 First Principles Simulations

The reduced thermal conductivity can be understood as a consequence of additional phonon scattering due to interface roughness. In the past, such interface roughness has been modeled under the particle picture of phonon transport as causing partially diffuse and partially specular phonon scattering at the interfaces [55], [66] or with molecular dynamics simulations [61]. Dr. Jivtesh Garg of Gang Chen's group at MIT performed first principles simulations on the thermal conductivities of GaAs/AlAs and Si/Ge SLs using density functional perturbation theory (DFPT), including the effects of atomic mixing at interfaces [44, 53, 111, 112, 113]. To compute the thermal conductivity from first principles, second-order and third-order interatomic force constants were derived using DFPT. The SL was then simulated by allocating the masses of Ga, Al, and As to the appropriate atoms in the unit cell. The calculation

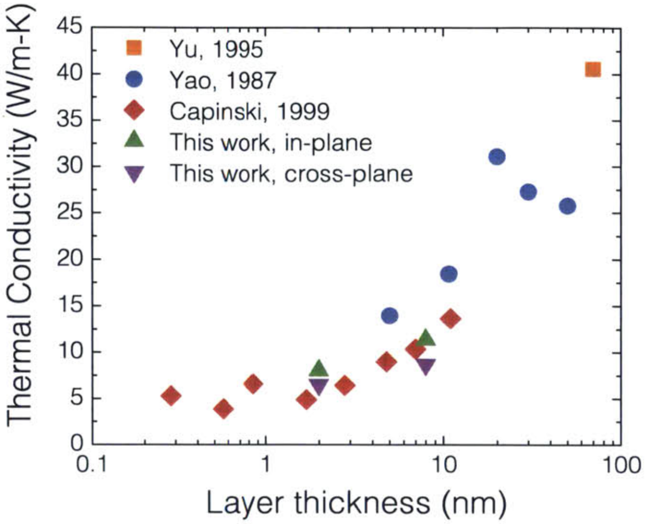

Figure 2-4: A comparison of the values of GaAs/AlAs thermal conductivities from the TDTR and TTG experiments with results from previous studies.

of in- and cross-plane thermal conductivities was performed both for SLs with perfect interfaces and SLs with atomistic mixing at interfaces but a fixed planarity. The atomistic mixing used in the simulations consisted of one monolayer on either side of the interface having randomly mixed Ga and Al atoms [114]. For perfect SLs, phonons scatter only through anharmonic 3-phonon processes and these scattering rates were computed using perturbation theory. Scattering from rough interfaces was computed by including random mass mixing in two atomic monolayers on either side of the interface. The thermal conductivities of the SLs were then calculated by solving the Boltzmann transport equation under the single-mode relaxation time approximation. Details of the simulation are published elsewhere [98]. The anisotropy was found to be higher in SLs with perfect interfaces (Fig. 2-5). The smaller anisotropy values for rough interfaces more closely corresponded to experimental values. The simulated anisotropy for a Si/Ge SL (2 nm x 2 nm) with interface mixing is approximately 2.3, in reasonable agreement with the experimentally determined value [111]. Furthermore, the results show why the thermal conductivity anisotropy of GaAs/AlAs

SLs is lower than that of Si/Ge SLs, where an increased mass mismatch leads to more scattering at the interfaces and a greater reduction in phonon group velocities. Due to computational power limits, the thermal conductivity of the 8 nm x 8 nm SL was not simulated. However, the experimental results for anisotropy are close to the simulated results for the 2 nm x 2 nm SL when atomistic mixing is included (Fig. 2-5).

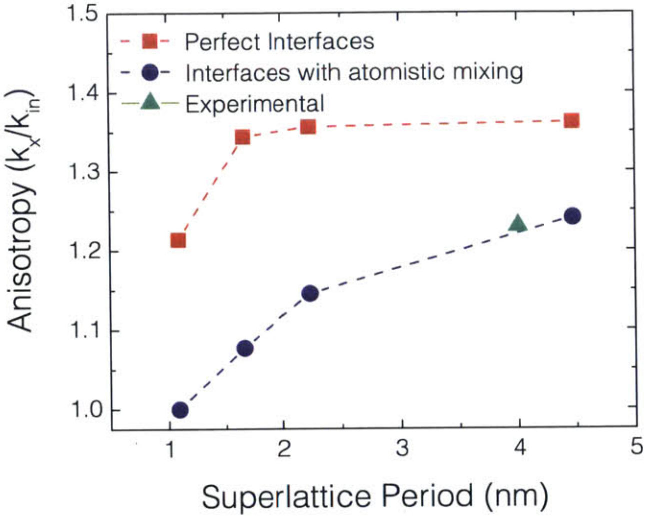

Figure 2-5: Anisotropy ratio of short period GaAs/AlAs superlattices. The ratio is lower when interfaces have atomic mixing and increases with increasing period.

However, the absolute values for the thermal conductivity from the simulations, both in the in-plane and the cross-plane directions, are approximately two times higher than the experimentally determined thermal conductivities (Table 1). This may be the result of the model used in the phonon DFPT simulation, wherein the interface roughness was approximated as random atomistic mixing, while real interface roughness in GaAs/AlAs SLs consists of both atomic mixing and local layer thickness fluctuations, also known as the formation of islands. The interface mixing is treated as a perturbation to perfect interfaces, essentially equivalent to that of point defects, resulting in a ω^4 frequency dependence of the scattering rates [98]. In this model, interface roughness predominantly affects high-frequency phonons while having little effect on the MFPs of low-frequency phonons. The local thickness fluctuations, which can have lateral dimensions 10 nm [115], can scatter long wavelength phonons. The additional island scattering picture is consistent with recent measurements of coherent phonon lifetimes in similar SL structures showing that extrinsic scattering rates of sub-THz phonons were indeed much larger than those predicted by the atomistic mixing model [116]. How to include both island formation and atomic mixing into DFPT simulations remains a challenge.

	SL layer thickness	
SL	2 nm	8 nm
GaAs/AlAs		
In-plane α_x (cm^2/s), experimental	0.0488	0.0693
In-plane k_x (W/m-K), experimental	8.05 ± 0.48	11.4 ± 0.46
In-plane k_x (W/m-K), calculated	18.64	
Cross-plane k_z (W/m-K), experimental	6.5 ± 0.5	8.7 ± 0.4
Cross-plane k_z (W/m-K), calculated	15.0	
Anisotropy, experimental	1.2 ± 0.12	1.3 ± 0.08
Anisotropy, calculated	1.24	
Si/Ge		
In-plane k_x (W/m-K), experimental	6.3	
In-plane k_x (W/m-K), calculated	9.35	
Cross-plane k_z (W/m-K), experimental	1.6	
Cross-plane k_z (W/m-K), calculated	5.02	
Anisotropy, experimental	3.9	
Anisotropy, calculated	1.9	

2.5 Summary

In summary, we have shown that the TTG technique is sensitive to the in-plane thermal conductivities of thin films, and combined it with the TDTR technique to probe the anisotropies in the thermal conductivities of GaAs/AlAs SLs. The anisotropy in the thermal conductivities of GaAs/AlAs SLs is much smaller than that of the Si/Ge SLs reported in the past, consistent with pictures obtained from first-principles simulation. Although DFPT simulations produced similar anisotropy values compared to experimental data for both GaAs/AlAs and Si/Ge SLs, the thermal conductivity values predicted are about a factor of two higher than experiments, potentially due to local thickness fluctuations.

Chapter 3

Coherent Phonon Heat Conduction in Superlattices

Most material reprinted with permission from M. N. Luckyanova, J. Garg, K. Esfarjani, A. Jandl, M. T. Bulsara, A. J. Schmidt, A. J. Minnich, S. Chen, M. S. Dresselhaus, Z. Ren, E. A. Fitzgerald, G. Chen, "Coherent Phonon Heat Conduction in Superlattices," *Science* **338** (6109), 936-939 (2012). Copyright 2012, AAAS.

The control of heat conduction through the manipulation of phonons as coherent waves in solids is of fundamental interest and could also be exploited in applications, but coherent heat conduction has not been experimentally confirmed, despite attempts to do so in a variety of nanostructures, as described in Chapter 1. In this chapter, we report the experimental observation of coherent heat conduction through the use of superlattices with a constant period thickness but varying numbers of periods. This is a departure from traditional experiments on SLs, where the period thickness was varied but the total thickness of the SL was kept constant. With this new experimental paradigm, we found that the thermal conductivity, measured with time-domain thermoreflectance (TDTR), increased linearly with increasing total superlattice thickness, which is consistent with a coherent phonon heat conduction process, as demonstrated in Chapter 1. First-principles and Green's functions-based simulations further support this coherent transport model.

3.1 Introduction

Heat conduction usually occurs via a random walk of thermal energy carriers such as phonons, electrons, or molecules. During the last two decades, size effects on phonon heat conduction that led to a deviation from this random walk behavior have drawn considerable attention [17]. Most experimental observations of phonon size effects can be explained by invoking the Casimir picture, wherein phonons travel ballistically or quasi-ballistically through the internal region of the specimen and scatter at interfaces and boundaries [15]. Such classical size effects are important for a wide range of applications including thermoelectric energy conversion and microelectronic thermal management.

In this classical size regime, the phase information carried by phonons is lost through the diffuse scattering of phonons at boundaries and by internal scattering processes (Fig. 3-1). However, it should be possible to control the conduction of heat by manipulating phonon waves through, for example, stop-band formation in periodic structures [31], soliton waves [76], and phonon localization [71]. Such manipulations require that heat-carrying phonons maintain their phase information throughout the heat conduction process. Coherent phonons in superlattices (SLs) have been observed with Raman scattering and acoustic reflection and transmission experiments, but these experiments probe a single frequency [59, 117, 118], rather than the integrated distribution associated with heat transfer. Thus, a conclusive demonstration of coherent phonon heat conduction remains an open challenge.

The term 'coherent' has different meanings in different fields. Typically, it is used to characterize the source of a nearly monochromatic wave and implies a measurable phase relationship for a given time interval during wave propagation. While this definition applies to a monochromatic wave, it does not apply to heat conduction, which involves all the thermally excited phonons in a structure. To clarify the meaning of coherent heat conduction, we consider heat conduction across the thickness of a thin film. In the Casimir classical size effect regime, broadband phonons thermally excited at one boundary traverse the internal region of the film ballistically. Upon reaching the sample boundary they are usually scattered diffusely (Fig. 3-1). Hence, phonon propagation inside the layer is coherent. However, because boundaries often scatter phonons diffusely, it is commonly assumed that such scattering randomizes the phases of phonons such that interference effects, and the resultant modification of the phonon dispersion, can be neglected. For a SL with many internal interfaces, the key question for heat conduction is whether each internal interface behaves as a diffuse boundary, as in the classical size effect regime, or whether it behaves as a new material with its own phonon dispersion caused by interference of phonon waves propagating through the whole structure. In the former case, phonon transport is incoherent and the SL can be thought of as a composite. In the latter case, phonon transport is coherent and the SL should be treated as one homogeneous material.

The idea of using periodic structures such as SLs and phononic crystals to control thermal transport by manipulating coherent phonons has existed for some time [50]. Past experimental and theoretical studies, particularly those of SLs, have made such control seem unattainable except at very low temperatures [50, 51]. For example, in SLs, extensive experimental and theoretical studies, which have focused on changing the periodicity, have shown that interface roughness and the resulting diffuse scattering play a dominant role in the experimentally observed thermal conductivity reduction compared to their bulk parent materials [28, 53, 54, 55, 56, 67, 119] implying that phonon transport through SLs is mainly incoherent. We now show that coherent heat conduction occurs in SLs, despite the dominance of diffuse interface scattering in reducing the phonon thermal conductivity. The issue of coherent versus incoherent transport is important for understanding energy transport in a variety of disciplines.

3.2 Experimental Approach

We have taken a different experimental approach to study heat transport through SLs. Rather than changing the thickness of the SL periods, we measure the thermal transport properties of SLs with a constant period but varying number of periods. If each internal interface scatters phonons diffusively, thus destroying their phase information, it behaves like a thermal resistor because of the Kapitza resistance [48], such that many equivalent interfaces in series lead to an effective SL thermal conductivity, in the direction perpendicular to the interfaces, that is approximately independent of the number of layers [55]. However, if the phase of the phonon is preserved at the interfaces of the SL and if anharmonic scattering is minimal, superposition of the Bloch waves creates stop bands and effectively modifies the phonon band structure [51].

In this regime, phonon mean free paths (MFPs) are equal to the sample length, leading to a thermal conductivity that is linearly proportional to the total thickness of the SL (Fig. 3-2). This SL structure has the equivalent of a constant conductance through all the layers [120], as would be expected in a thin film with no internal scattering. In the case of a single material system, this regime is typically referred to as the 'ballistic' transport regime. In the case of SLs, this implies that these phonons are eigenmodes of the SL and therefore have the modified dispersion arising from coherent wave interference effects. Therefore, in the case of SLs, ballistic transport across the whole thickness means coherent heat conduction in the SL. We should

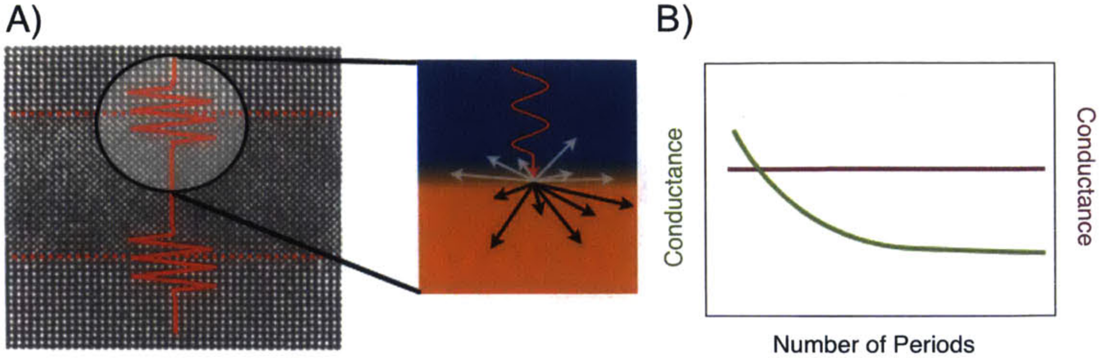

Figure 3-1: (A) In the incoherent transport picture, the phonons travel ballistically, without scattering, through the internal layers of the SL, but scatter diffusively at each interface. (B) This results in a constant thermal conductivity with increasing number of periods, as expected from any bulk material.

caution not to equate ballistic heat conduction to coherent heat conduction in general, as ballistic heat conduction is widely used to describe reduced thermal conductivity of nanowires caused by diffuse scattering of phonons at the boundaries [30].

3.2.1 Sample preparation

We used metal-organic chemical vapor deposition (MOCVD) to fabricate five GaAs/AlAs SL samples consisting of 1, 3, 5, 7, and 9 periods, where each period consists of 12 nm of GaAs and 12 nm of AlAs (Fig. 3-3(A)). The superlattice (SL) samples were prepared using metal organic chemical vapor deposition (MOCVD) on undoped GaAs wafers oriented in the (001) direction. Prior to the SL growth, a 500 nm GaAs buffer layer was grown on the substrate. Cross-sectional transmission electron microscope (TEM) images of the samples, such as Fig. 3-3(B), were used to confirm the thickness of the layers and high-resolution (HR) TEM images such as the inset in Fig. 3-3(B) confirmed the good quality of the interfaces between the layers. High-resolution TEM images have low contrast for dilute concentrations of GaAs in AlAs and vice versa, which makes determining the exact amount of interfaces mixing somewhat difficult.

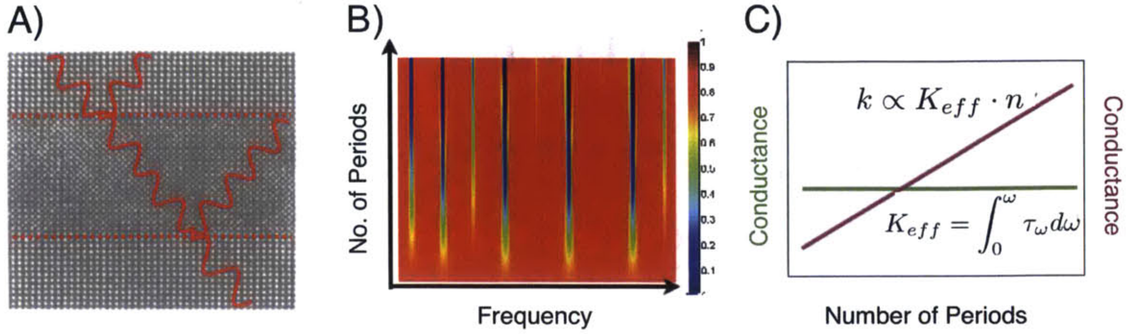

Figure 3-2: Specular reflection and transmission of phonon waves at interfaces leads to coherent interference of Bloch these waves. (B) As the length of the sample, or the number of periods, increases, there is a buildup of these interference effects, leading to the formation of transmission bands and stop bands, where some frequencies do not propagate. (C) Integrated over all frequencies, these stopbands, which have a negligible effect in the GaAs/AlAs material system, leads to a constant thermal conductance with number of periods, and a resultant linearly increasing thermal conductivity.

Recent scanning transmission electron microscopy (STEM) studies of MBE grown GaAs/AlAs SLs have found interface mixing to extend over three atomic layers [114]. The samples used in this study are expected to have slightly greater mixing due to the higher temperatures used in MOCVD. An aluminum layer was deposited using electron beam evaporation on the SL samples, on a sapphire sample, and on a piece of the GaAs substrate using electron beam evaporation. The thickness of the Al layer was measured using profilometry and verified with time-domain thermoreflectance (TDTR) measurements of the sapphire calibration sample. Both techniques yielded Al layer thicknesses within a 5 nm window of 100 nm.

3.2.2 Measurements

We used time-domain thermoreflectance (TDTR) measurements to find the thermal conductivities of these samples [54, 83] at temperatures between 30 K and 300 K. The samples were mounted into a cryostat under high ($\sim 10^{-5}$ torr) vacuum and

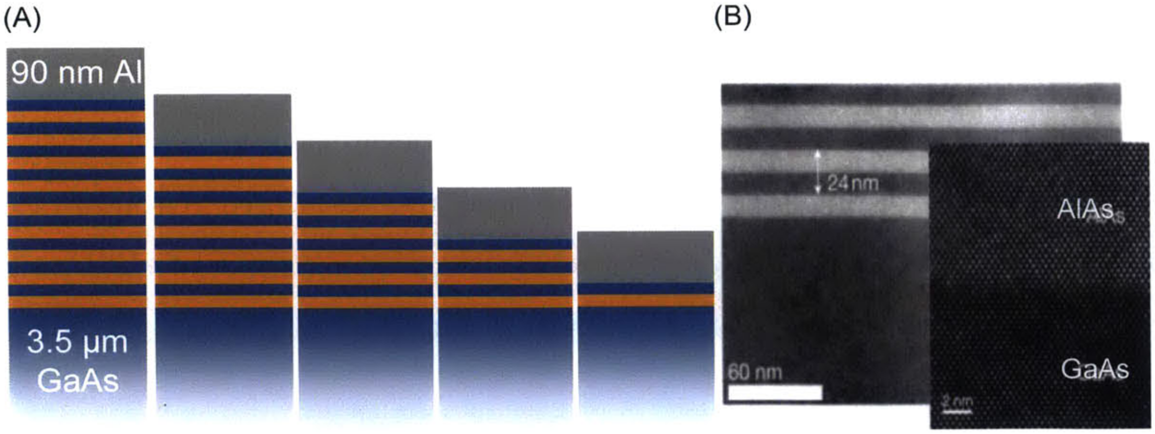

Figure 3-3: (A) Five samples were fabricated on GaAs substrates, 12 nm GaAs x 12 nm AlAs SLs of 1, 3, 5, 7, and 9 periods. Each sample was coated with 90 nm of Al to facilitate TDTR measurements. (B) X-TEM images confirmed the thickness of the SLs and X-HRTEM images confirmed the high quality of the interfaces.

were cooled using liquid He for low-temperature measurements. The temperature of the sample was measured using a Si diode in contact with the surface of the sample via thermal grease. The TDTR experimental setup used herein was discussed in greater details in the relevant references [68, 85].

The results of the thermal conductivity measurements represent the averages of approximately 60 individual thermoreflectance curves. Three thermoreflectance measurements were performed at five locations on each sample and at four different modulation frequencies: 3, 6, 9, and 12 MHz. No modulation frequency dependence was observed in the data, so all the data from the different frequencies were included in the averaging. In general, the standard deviation from the average is approximately 10%.

The cooling curve yielded by the experiment was fitted to the solution of the Fourier heat conduction equations applied to a multi-dimensional, multi-layer stack to determine the unknown parameters. In this case, the unknown parameters were the thermal interface conductance (TIC) between the Al optical transducer layer and the SL and the thermal conductivity, k, of the SL. The average of the heat capacities of AlAs and GaAs were used for the heat capacity of the SL. Separate measurements of the thermal properties of Al on a GaAs substrate provided an initial guess for the TIC. The interface conductance, which is highly dependent upon the sample quality, the deposition quality, and the sample surface chemistry, was allowed to float to yield best fitting results. In order to determine whether the interface conductance was greatly affecting the results of the experiment, a sensitivity analysis was performed (Fig. 3-4) [121].

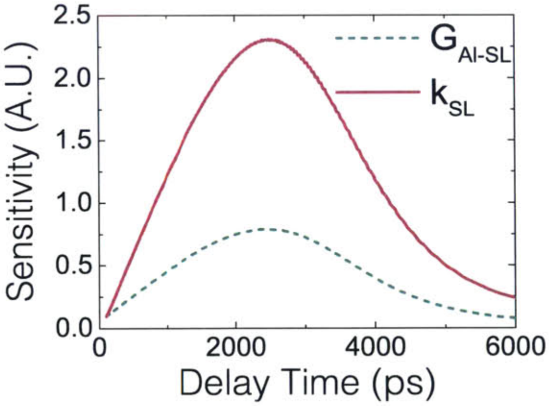

Figure 3-4: Sensitivity analysis for a 1-pd SL sample at 30K. This analysis shows that for all times, the fitting is more sensitive to the thermal conductivity of the SL rather than the thermal interface conductance.

For the thinnest sample at the lowest temperatures, where the interface conductance was expected to play the largest role, a representative sensitivity analysis is shown in Fig. 3-4. This analysis shows the sensitivity of the fitting of a 1-pd SL to both the thermal conductivity of the sample and the TIC at 30K and a modulation frequency of 6 MHz. The plot shows that the fitting is more sensitive to the thermal conductivity of the sample for all times. This result is understandable when one considers the dependence on heat capacity of the solution to the heat equation. The interface has no heat capacity while the layer itself has a finite heat capacity.

To further verify these sensitivity results, we plot the data along with best fit lines (in blue) as well as lines of variation (in red and green for +/- variations) in Fig.

3-5(A) and Fig. 3-5(B). These lines of variation show how much the fitting curve would change with a prescribed change in the value of a specific fitting parameter. Figure 3-5(A) shows that with a 100% change in the interface conductance, the fitting curve does not change. However, Fig. 3-5(B) shows that with just a 10% change in the thermal conductivity of the sample, the fitting curve does change. This analysis further verified that the fitting was more sensitive to the thermal conductivity of the SL rather than the TIC, thus providing confidence in the results of the experiment presented in the paper.

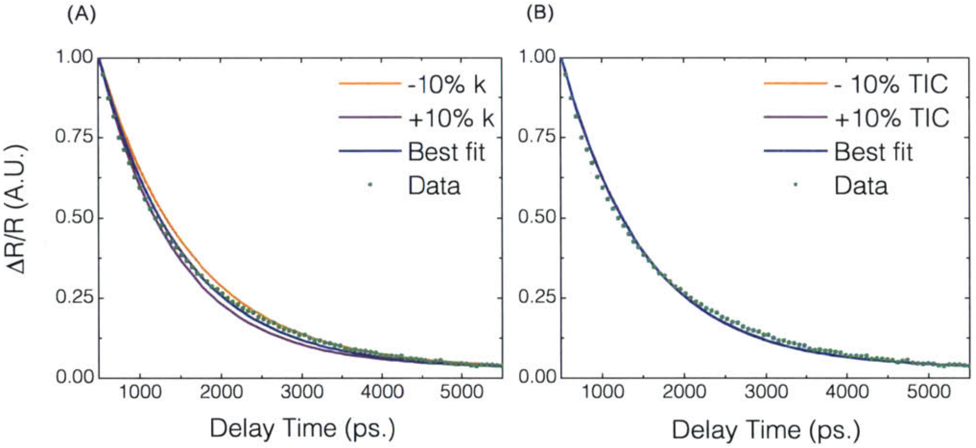

Figure 3-5: (A) Data for a 1-pd SL sample at 30K and 6 MHz pump modulation frequency. The teal crosses are data points, the blue line represents the line of best fit, the green and red solid lines are the best fit lines if the SL thermal conductivity is varied by +/-10%. (B) Data for the same sample as in (A) where, again, the blue line represents the line of best fit and the red and green lines represent the lines of best fit if the Al-SL thermal interface conductance is varied by +/-100%.

We should acknowledge that strictly speaking, fitting the experimental data using Fourier theory is not valid. Instead, the Boltzmann equation should be solved using scattering rates and phonon transmissions as input parameters. Such computations, however, are beyond current computational abilities. Past studies of one-dimensional pump-and-probe setups show that the Boltzmann equation can be fitted reasonably well by Fourier's law using a reduced thermal conductivity [122].

In the worst-case scenario for our experiment (300 K for the 9 period SLs), we estimate that about 40% of the total thermal conductivity is contributed by ballistic phonons with frequencies below 1 THz, and they traverse the SL in 0.2 ns, which is much shorter than the 6 ns experimental time. The other 60% is contributed by diffusive phonons that can be reasonably described with the diffusive Fourier law. This explains why the Fourier law calculation can fit the experimental data reasonably well, as shown in Figs. 3-5(A) and 3-5(B). The effective thermal conductivity values extracted from the experimental study are used together with first-principles and Green's functions simulations to reveal the coherent phonon transport mechanism.

3.3 Experimental Results

The thermal conductivities of the SL samples resulting from the TDTR experiment are given in Figs. 3-6(A) and 3-6(B). The conductivity was linear in total SL thickness from 30K to 150 K (Fig. 3-6(A)). This nearly linear dependence of thermal conductivity on number of SL periods implies coherent phonon transport through the layers, whereas the nonlinear dependence at temperatures greater than 150 K suggests the increasing influence of incoherent effects. However, because the thermal conductivity was still increasing with period number even at 296 K, coherent phonons still conduct a considerable fraction of heat at this temperature. The effective thermal conductivities of these SLs are much smaller than that of their bulk counterparts (room temperature thermal conductivity of GaAs is 45 W/m-K and that of AlAs is 90 W/m-K [123]) and are increasing with temperature.

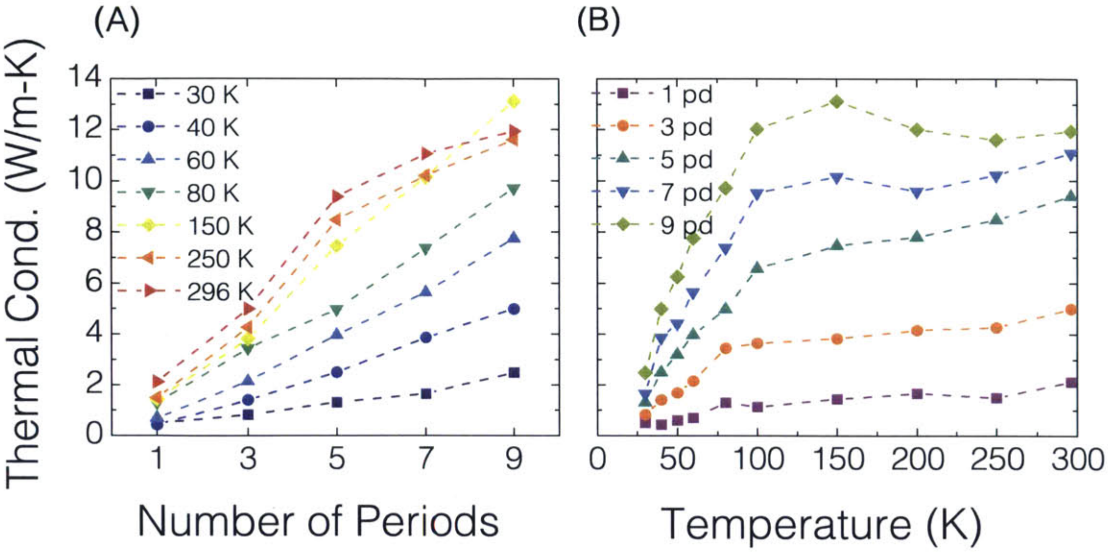

Figure 3-6: Measured thermal conductivity of GaAs/AlAs SLs as a function of (A) number of periods in the SL for different temperatures and (B) temperature for different SL thicknesses. If the interfaces in the SLs destroy the phonon coherence, the measured thermal conductivity is expected to be independent of the number of periods. Below 150K, the linearity of the thermal conductivity versus length suggests that phonon heat conduction in these SLs is coherent.

3.4 Simulations

3.4.1 First principles simulations

To understand the experimental results, we used a first-principles approach based on lattice dynamics to calculate the phonon MFPs of an infinite SL at different temperatures. These simulations were performed by Dr. Jivtesh Garg of Gang Chen's group at MIT. Unlike past theoretical approaches based on the Boltzmann transport equation [55], lattice dynamics [61, 65], molecular dynamics [97, 119, 124] and acoustic wave equations that relied on various assumptions and fitting parameters, our first-principles approach relies upon the use of harmonic and anharmonic interatomic force constants derived from density-functional perturbation theory (DFPT)

[125] along with a solution of the Boltzmann transport equation to predict the thermal conductivity. Its use has been shown to lead to excellent agreement between experiments and theory for perfect crystals [44, 126] as well as alloys [112]. Garg *et al.* [64] used this approach to compute the thermal conductivity of ideal Si/Ge SLs with perfect interfaces where phonons were taken to scatter only through anharmonic processes. The computed thermal conductivity values were higher than experimental values, indicating the need to incorporate the effects of interfacial disorder.

In the first-principles formalism the thermal conductivity of GaAs/AlAs SLs is computed by solving the Boltzmann transport equation in the single mode relaxation time (SMRT) approximation using Eq. 3.1 below. The thermal conductivity was computed by summing over the heat conducted by all the phonon modes (λ) in the Brillouin zone:

$$k_\alpha = \frac{h^2}{N\Omega k_B T^2} \sum_\lambda c^2_{\alpha\lambda} \omega^2_\lambda \bar{n}_\lambda (\bar{n}_\lambda + 1) \tau_\lambda \tag{3.1}$$

where c, ω, $\bar{n}$, and τ are the phonon group velocities, frequencies, equilibrium populations, and relaxation times, λ represents the vibrational mode labeled by (q_j) (q is the wave vector and j the phonon branch), and T, Ω, and N are the temperature, cell volume, and size of the q-point mesh used. The scattering rate, $1/\tau_{lambda}$, of a phonon mode λ is taken to be the sum of a term describing scattering due to interfacial disorder $(1/\tau_{\lambda a})$ and a term describing anharmonic scattering $(1/\tau_{\lambda b})$ as in Matthiessen's rule.

All ingredients necessary to compute the thermal conductivity, namely the phonon frequencies, group velocities, populations and lifetimes, are derived from first-principles using density functional perturbation theory (DFPT). The second order and third order interatomic force constants needed to estimate the above parameters are taken to be an average of those in pure GaAs and AlAs and these constants are also obtained from DFPT.

The anharmonic scattering rates ($1/\tau_{\lambda b}$) are computed using the lowest-order three-phonon scattering processes in the SMRT approximation via [127]

$$\begin{aligned}\frac{1}{\tau_{\lambda b}} = \pi \sum_{\lambda'\lambda''} \mid V_3(-\lambda, \lambda', \lambda'') \mid^2 \times [2(\bar{n}_{\lambda'} - \bar{n}_{\lambda''})\delta(\omega(\lambda) + \omega(\lambda') - \omega(\lambda''))+ \\ (1 + \bar{n}_{\lambda'} - \bar{n}_{\lambda''})\delta(\omega(\lambda) - \omega(\lambda') - \omega(\lambda''))\end{aligned} \tag{3.2}$$

where $V_3(-\lambda, \lambda', \lambda'')$ is the three-phonon coupling matrix elements or the weighted Fourier transforms of the cubic force constants.

Interface roughness is simulated as a random mixing of Ga and Al atoms in a narrow region around the interface; this mass-mixing is the dominant interfacial scattering mechanism for phonons at short periods [85, 128]. To compute the interfacial scattering rates, we replace the disordered crystal with an ordered one and treat the disorder as a perturbation [129] (an idea first proposed by Abeles [130] for alloys); the use of perturbation theory to compute scattering rates due to mass disorder has been found to yield excellent agreement with experiments [131]. In this perturbative approach, for any SL unit cell the masses of the atoms at sites affected by the disorder are taken to be an average of Ga and Al masses, and the other atoms on either side of the interface are assigned their true masses. We take the thickness of the disordered region to be two layers total consisting of one layer of AlAs and one layer of GaAs with random mixing of Ga and Al atoms. This assumption is consistent with HRTEM images, such as Fig. 1A, and with previous microscopy studies of GaAs/AlAs interfaces [85]. The phonon modes of this unit cell are used to compute the frequencies, group velocities, populations and lifetimes that enter into the calculation of the thermal conductivity. The scattering rates due to interfacial disorder are calculated using:

$$\frac{1}{\tau_{\lambda a}} = \frac{\pi}{2N}\omega_\lambda^2 \sum_{\lambda'} \delta(\omega_\lambda - \omega_{\lambda'}) \sum_{\sigma} g(\sigma) \mid^r e(\sigma \mid \lambda')^r e(\sigma \mid \lambda) \mid^2 \tag{3.3}$$

where σ denotes the atomic sites in the SL unit cell, g takes into account the magnitude of the mass disorder and is defined as $g(\sigma) \doteq \sum_i f_i(\sigma)[1-m_i(\sigma)/\bar{m}_i(\sigma)]^2$ where i, f, and m denote the atomic species, concentration and mass, respectively, and $\bar{m}(\sigma)$ is the average mass at site σ and e represents the vibration eigenvector. The non-zero only for atomic sites in the region of disorder is $g(\sigma)$. The above equation therefore allows us to compute the phonon scattering due to sub-lattice disorder which is the vase for interfacial disorder.

The harmonic force constants are obtained on a 10x10x10 supercell, respectively. The anharmonic force constants are obtained by using a supercell approach as outlined by Esfarjani *et al.* [132]. For all DFPT calculations, a 8x8x8 Monkhorst-Pack [133] mesh is used to sample electronic states in the Brillouin zone and an energy cutoff of 72 Ry is used for the plane-wave expansion. We carefully tested the convergence of all measured quantities with respect to these parameters. First-principles calculations within density-functional theory are carried out using the PWscf and PHonon codes of the Quantum-ESPRESSO distribution [35] with norm-conserving pseudopotentials based on the approach of von Barth and Car [134]. Thus, in this work, we include both interface roughness as the random mixing of Ga and Al atoms in a narrow region around the interface, and three-phonon processes from first principles without introducing any fitting parameters. Scattering caused by this mixing was computed from the Fermi golden rule [129].

The above formalism was first used to compute the thermal conductivity of SLs with periods 1.1, 1.6 and 2.2 nm. Calculation of phonon scattering rates beyond a period of 2.2 nm was found to be prohibitively expensive. To compute the thermal conductivity of the 24 nm period SL, we took the anharmonic rates to be the same as in the 2.2 nm SL, since they were found to remain unchanged as the period was increased from 1.6 to 2.2 nm. The interfacial scattering rates, however, were found to scale inversely with the period; for the 24 nm period SL these were therefore obtained by scaling the rates computed for the 2.2 nm period SL.

Figure 3-7 shows the phonon dispersion along the thickness direction of the 12 nm x 12nm GaAs/AlAs SL. Only lower frequency phonons are shown. In this region, according to Fig. 3-8, interface scattering is weaker than phonon-phonon scattering and phonon transport across the measured SLs is ballistic. The coherent effects are reflected in the minigaps and modified group velocity of the phonons in the SLs.

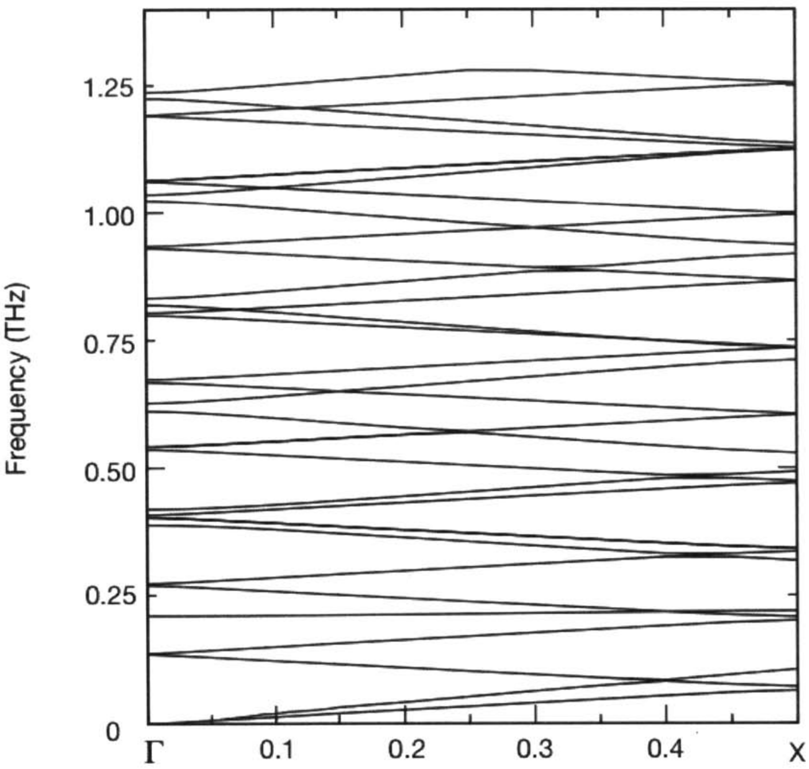

Figure 3-7: Phonon dispersion of the 24 nm period GaAs/AlAs superlattice along $\Gamma - X$. Only low frequency phonon modes are shown. This dispersion which incorporates the coherence effects as indicated by the phonon band gaps is used for computing the thermal conductivity.

Based on the results from these first-principles computations, we can extract detailed information such as the phonon MFP distribution and the MFP dependence of the thermal conductivity. Although these calculations were performed for an infinite SL, the information obtained regarding phonon MFPs allowed us to gain insight into the role of coherent transport in finite-size SLs. Figure 3-8(A) shows the anharmonic and interface scattering rates at different frequencies. Although lower frequency phonons were mostly scattered through three-phonon processes, higher frequency phonons were also scattered by the interfacial disorder. This interfacial scattering of high-frequency phonons led to a reduction in their heat-carrying ability and caused an overall decrease in the thermal conductivity of SLs. Low-frequency phonons had long MFPs (Fig. 3-8(B)) and could propagate through the entire SL structure and thus conduct heat coherently through a SL whose thickness was shorter than the MFPs.

The contribution of these long MFP phonons to the total thermal conductivity is shown in Figs. 3-8(C) and (D), where thermal conductivity accumulation is plotted against MFP and frequency, respectively. Phonons with MFPs longer than 216 nm, the thickest measured SL, contributed 87% (at 100K) and 71% (at 300K) to the total thermal conductivity of an infinite SL, as indicated by the dashed lines in Fig. 3-8(C). This finding points to the important role that low-frequency, long MFP phonons played in heat transport through SLs. These phonons form a new band structure with altered group velocities (Fig. 3-8) and stop bands.

3.4.2 Green's functions simulations

Further evidence of the dominant role of coherent phonon transport in finite SLs is provided by a Green's function (GF) based calculation of the SL thermal conductivities [135, 136, 137]. This theory is purely harmonic but rigorously includes roughness effects and the finite thickness of the SLs. Because first principles results have shown that most of the heat is conducted by low-frequency phonons that are only weakly scattered by anharmonic processes in the bulk, we expect the GF treatment, which ignores this anharmonicity, to be valid [65]. The experimental results indicate that for the finite thickness SLs, phonon transport was mostly coherent. In this regime, similar to the Casimir regime, the thermal conductivity of the SL was mainly determined

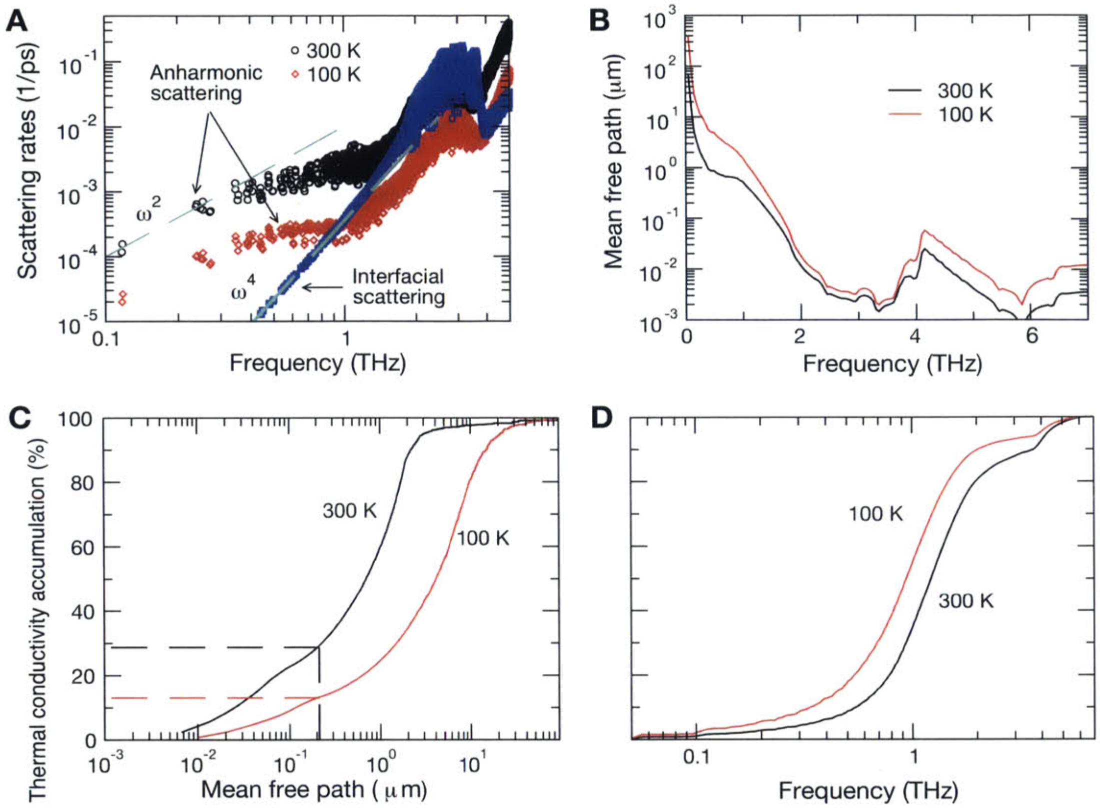

Figure 3-8: Calculated first-principles results for an infinite 12 nm x 12 nm GaAs/AlAs SL (A) Comparison between anharmonic (red for 100K and black for 300K) and interface (blue) scattering rates. Dashed green lines are the fits to the scattering rates describing the ω^2 and ω^4 behaviors of the anharmonic and interfacial scattering, respectively, in the low-frequency regime. (B) Phonon MFPs in the SL as a function of frequency. Thermal conductivity accumulation in the SL as a function of (C) phonon MFP and (D) frequency, at 100K and 300K.

by scattering at the sample boundaries rather than at internal interfaces.

The thermal conductance of the superlattice structure is calculated using the Landauer formula [120] based on the transmission function. The latter is calculated using the Green's function (GF) formalism detailed in [136, 137]. Fast algorithms are used [138, 139] to compute the effects of the GaAs substrate and the Al capping layer which are both considered as semi-infinite leads (Fig. 3-9(A)). Since the considered model is harmonic, three-phonon processes are excluded and thus it is assumed that the total thermal resistance comes from phonon scatterings at interfaces due either to roughness or acoustic impedance mismatch. When this formalism is applied to phonons, the energy argument E needs to be substituted by the square of the phonon frequency ω^2, and the Hamiltonian matrix by the force constant matrix. Due to the translational invariance of the system along the transverse direction, the harmonic problem can be decoupled into N independent chains, one for each considered transverse k vector. The resulting formula for the thermal conductance becomes:

$$G_{ballistic} = \sum_{m,k_t} \frac{1}{N} \int_0^{\inf} \frac{d\omega}{2\pi} C_v(\omega/T)\Xi_m k_t, \omega) = \kappa \frac{A}{L} \tag{3.4}$$

where C_v is the heat capacity per mode ($C_v = \hbar\omega(\delta n/\delta T)$) with $x = \hbar\omega \; 2k_B T$) and Ξ is the transmission function of a phonon of frequency ω and transverse momentum k_t

We show the phonon transmission function across a 5- and 9- period SL sandwiched between semi-infinite Al and GaAs leads where both clean and rough SL interfaces are considered. Low-frequency phonons were not affected by interface roughness (Fig. 3-9(B)) because their wavelengths were longer than the scale of the roughness. However, high-frequency phonons had a lower transmission as the SL became longer. At low frequencies, the transmission did not vary much with sample thickness. Figure 3-9(C) shows the thermal conductivity of the SL versus length for samples with rough interfaces. Because the transmission depended on the roughness conditions of the SL sample boundaries, which are difficult to predict due to the polycrystalline nature of the Al film, an exact match between experiments and simulation was not expected. Nevertheless, the temperature dependence of the thermal conductivity in the dominantly coherent regime (T<100K) was consistent between the experiments and the GF calculations. To obtain reasonable numerical agreement with experiments, the force constants between the Al layer and the SL were reduced and their masses were increased so as to artificially increase the interfacial thermal resistance by an order of magnitude. In actual experiments, it was found that this interfacial resistance depends highly on environmental and sample preparation conditions, which justifies such a treatment.

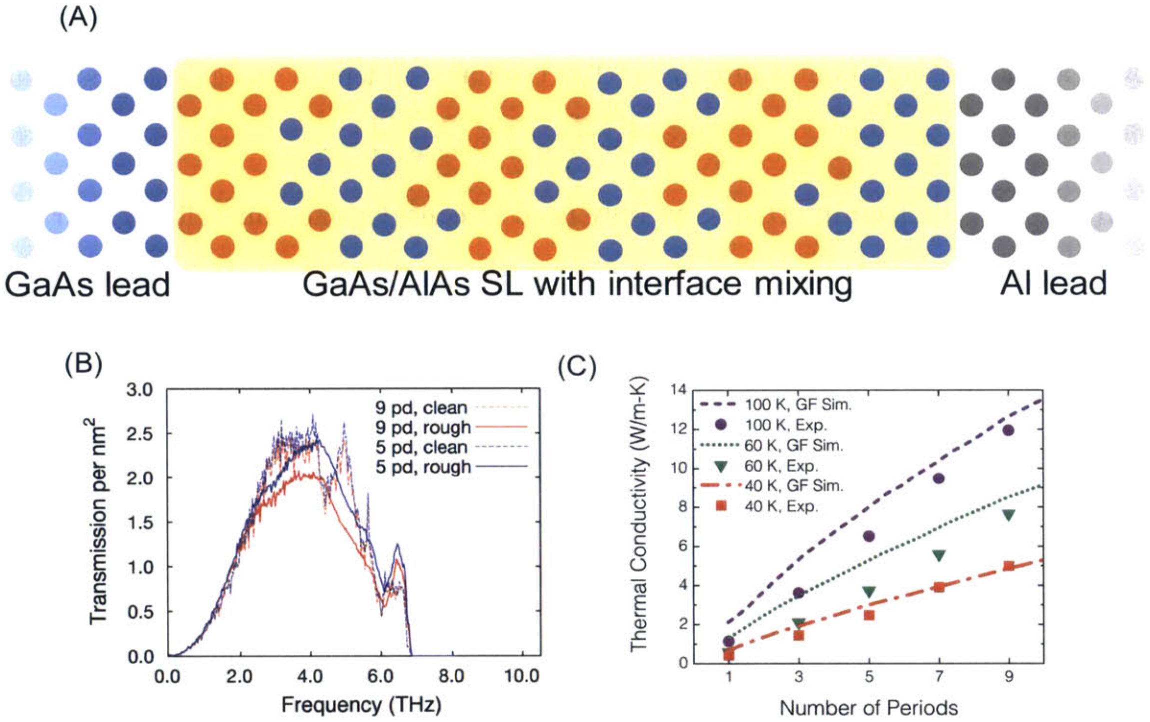

Figure 3-9: (A) Schematic representation of the input structure for the Green's functions calculations. (B) Transmission function per nm^2 of the 5- and 9-period SLs in the clean and rough boundary cases. (C) Thermal conductivity as a function of length at 40K, 60K and 100K for an SL with rough interfaces (solid) and experimental samples (dots with error bars).

In Fig. 3-9(B), the transmission function is divided by the cross section area of the considered 3x3 supercell, and summed over all transverse modes, in order to get the total transmission at a given frequency, per unit area. In the limit of elastic scattering, the transmission function is given by:

$$\Xi(k_t, \omega) = Tr[G\Gamma_L G^\dagger \Gamma_R] \tag{3.5}$$

In this formula, G is the GF of the whole system projected on the SL volume, and the Γs are the escape rates to the left (GaAs) or right (Al) leads. To convert conductance to conductivity, we multiply the former by the system length and divide by its cross section area. To model rough interfaces, we consider one unit cell on the left and one unit cell on the right of the interface, and randomly shuffle their Al and Ga atoms, while maintaining the As atoms at their original positions. This shuffling therefore covers a thickness of about 1 nm, given that the unit cell length on each side is about 0.54 nm.

In the case of clean interfaces, we only need to consider one unit cell in the transverse direction and we perform the summation over k_t defined on a fine mesh (30x30). The cross sectional area of the unit cell is 0.38 nm x 0.38 nm. For rough interfaces, where Ga and Al atoms are randomly shuffled within a layer of the interface, the adopted transverse cell is 3x3 (9 times larger), and the summation is over a 10x10 k_t mesh. In addition, we perform an averaging of the obtained transmissions over 9 sets of randomly generated atomic configurations. We also performed similar calculations for a 6x6 transverse cell and did not see any difference in the average transmissions, and we therefore kept the supercell size of 3x3 for the rest of the calculations.

For the calculations of the force constants (FC) appearing in the Green's functions, we adopted a simple two-nearest neighbor FC model for all three materials: GaAs, AlAs, and Al. It produced a very reasonable band structure and phonon density of states for these materials with the correct bandwidth. The speeds of sound were however off by 10-20% depending on the considered material and direction. The obtained DOS and transmission function can be seen in Fig. 3-10.

The reason for using semiempirical force constants as opposed to first-principles ones was simply their ease of use. In case we need to artificially modify the force constants or make the correct connection of the Al lattice to GaAs which has a different coordination number, the use of an analytical formula is much more convenient. Even though our goal here was not to get exact quantitative agreement with the experiment but was instead to show qualitatively the trends, the used force constants yield very reasonable band structure and transmission values. The transmission calculations

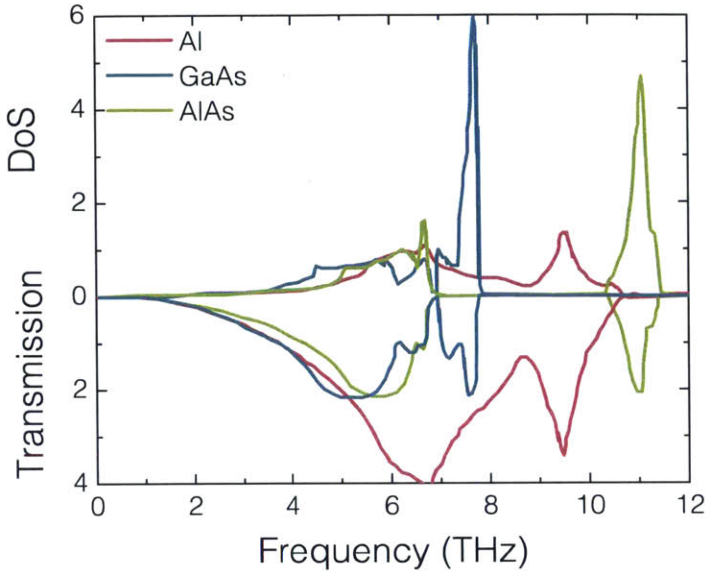

Figure 3-10: Phonon density of states (top) and negative of the transmission function (bottom) for the three considered bulk structures. For an ideal infinite system, the transmission is essentially the DOS multiplied by the group velocity in the transport direction (100). For clarity, the transmission function has been plotted below the x axis. It is the total transmission within a 0.38 nm x 0.38 nm unit cell, summed over all transverse momenta.

were done for a size similar to the real experiment: SLs of 1, 3, 5, 7, 9 periods were made, in which each period consisted of 22 unit cells of GaAs and 22 unit cells of AlAs, resulting in a period of 23.76 nm containing 176 atoms per unit cell.

3.5 Summary

Our experimental and theoretical studies show that most of the phonons that contributed to the measured thermal conductivity in SLs traversed the SLs ballistically and hence were coherent. Interface roughness was effective in destroying the coherence of high frequency phonons, but not effective in scattering low-frequency phonons. The large reduction in thermal conductivity resulted from the loss of coherence of high frequency phonons, but the lower frequency phonons that contribute to the thermal conductivity were mostly coherent during their transport through the SL structures until they are scattered at the sample boundaries.

This conclusion has important implications on the future of phonon engineering. For thermoelectric applications, for example, a lower thermal conductivity can be achieved if the coherence of these low-frequency phonons can be broken. The coherence of long wavelength phonons can be destroyed by introducing perturbations that vary over long length scales. Examples of such perturbations are the strain associated with dislocations, and aperiodic SLs. Indeed, some past experiments show that quantum-dot SLs [140], metal-dielectric SLs [141], and disordered layered crystals [142] exhibit very low thermal conductivity that may have been the result of the destruction of long-wavelength phonon coherence. With the identification of the contribution of coherent phonons to heat conduction, we expect that novel strategies can be developed to further suppress or enhance the thermal conductivity of nanostructured materials.

Chapter 4

Breaking Phonon Coherence in Superlattices: Phonon Localization in Heat Conduction

In this chapter, we expand on the results of the previous chapter where coherent phonon heat conduction was observed in SLs with constant period thicknesses but changing numbers of periods. The previous chapter's simulations and recent experiments revealed that, in SLs, most phonons responsible for heat conduction have long wavelengths because short wavelength phonons are strongly scattered at individual interfaces [55, 61, 143]. The residual heat is carried by long-wavelength phonons that traverse the entire SL and obey its dispersion relation. In this chapter, we aim to scatter these long-wavelength phonons as well, further reducing the thermal conductivities of SLs. The phonons responsible for heat conduction in most dielectrics and semiconductors have short wavelengths. Although studies on phonon heat conduction in nanostructures over the past two decades have demonstrated the presence of strong size effects, most experimental observations of the departure from bulk behavior can be explained without invoking the wave nature of phonons [18, 30, 144, 145].

Instead, the classical size effects happen when the phonon mean free paths (MFPs) are longer than the characteristic sizes of the structures, and they are important for a wide range of applications including thermoelectric energy conversion and microelectronic thermal management [26, 69, 88, 146, 147]. As mentioned in Chapter 1, the potential of engineering phonon heat conduction via wave effects like bandgap formation [31, 50, 148, 149], solitons [76], or localization [150, 151] has been suggested before, but conclusive experiments have been lacking until the demonstration of coherent phonon heat conduction [98, 152] in superlattices (SLs) described in the previous chapter. In this chapter, we demonstrate the ability to control these long wavelength phonons by placing nanoscale dots at the interfaces of the SLs, leading to a further reduction of SL thermal conductivity by over a factor of two. Furthermore, our experiments demonstrate localization of long wavelength phonons, establishing a new paradigm for engineering phonon heat conduction in solids.

4.1 Experimental Approach

In the SL system, high-frequency phonons are primarily scattered by interface roughness and atomistic mixing. Since the length scale of interface roughness is usually too small to effectively scatter long-wavelength phonons, they are instead dominantly scattered through anharmonic processes. When the MFPs of these low-frequency phonons are longer than the entire sample length, they are scattered at the boundaries of the SLs rather than at the internal interfaces between layers. These propagating phonons represent eigenstates of the SL rather than of the parent material. Such coherent phonon transport has been previously observed in GaAs/AlAs SLs where the period thickness was held constant while the number of periods, and thus the overall sample thicknesses, was varied [98] as described in the previous chapter. The thermal conductivity of these SLs depends on the total thickness of the SL. This effect was especially pronounced at lower temperatures, where long-wavelength phonons dominate thermal transport. By introducing scatterers with sizes comparable to the wavelengths of these phonons, further reduction in thermal conductivity is expected. It will be especially interesting if these long-wavelength phonons can be localized.

4.1.1 Sample preparation

We fabricated three sets of seven SLs, with 4, 8, 12, 16, 100, 200, and 300 periods comprising a 3 nm GaAs layer and a 3 nm AlAs layer on a semi-insulating GaAs [001] substrates. GaAs/AlAs superlattices (SLs) with ErAs nanoparticles are grown epitaxially [153, 154]. All the samples were grown in a Veeco Gen III MBE system. Solid source materials Ga, Al, Er and a Veeco valved cracker for As were used for the growths. Sub-monolayer (ML) ErAs deposition was inserted at each GaAs/AlAs interface and the two surface coverages of 8% and 25% were aimed by 0.32 ML and 1 ML ErAs deposition, respectively. Depositions of ErAs are described in MLs as if the ErAs had grown in a layer-by-layer growth mode (1 ML of ErAs = 2.87 Å of film thickness). The growth rates of GaAs and AlAs were set to be around 1 μm/hr while the ErAs growth rate was kept at 0.02 ML/sec. The As_2 overpressure was maintained at 8x10-6 torr during the growth. All the samples were finished with a 3 nm GaAs layer to prevent possible oxidation of either AlAs or ErAs. ErAs has a lattice constant of 5.74 Å while that of GaAs is 5.6533 Å, a mismatch of 1.53%. In general, we believe the growth rate calibration of ErAs can have a variation of a few percentages. And we estimate the surface coverage by dividing the ErAs layer thickness (from the growth rate calibration) by 4 monolayers (which was observed from previous TEM studies showing that most of the ErAs dots tend to form 4 ML tall). TEM images of the different sample configurations are shown in Fig. 4-1.

The three sets are distinguished by the content of ErAs dots with an approximate diameter of 3 nm grown at the interfaces: (1) a reference set without dots at the interfaces (hereon referred to as the reference set), (2) a set with 8% (by area) interface surface coverage, leading to a spacing of about 9.5 nm between islands and (3) a set with 25% interface coverage, with an approximate inter-dot spacing of 5.5 nm. A schematic diagram of the SLs as well as TEM and HRTEM images of the samples are shown in Fig. 4-1. The images confirm the quality and consistency of the SLs, and the random distribution of the dots at the interfaces.

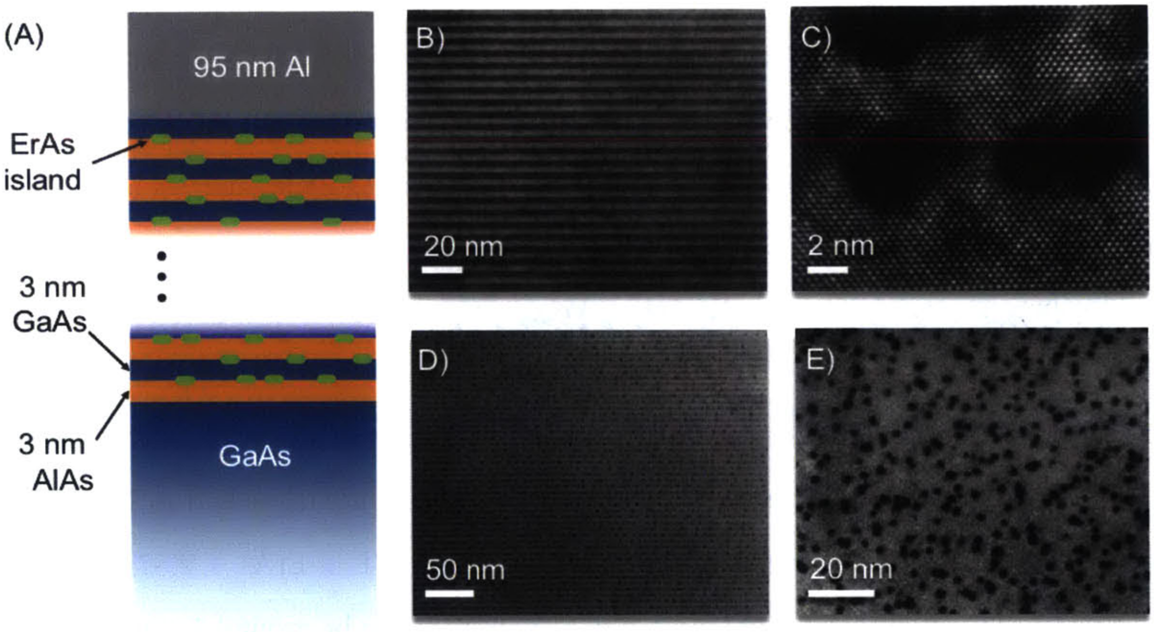

Figure 4-1: (A) Illustration of the superlattice samples. All samples have a fixed period thickness (3 nm of GaAs and 3 nm of AlAs) with varying numbers of periods. Three sample sets are distinguished by a varying ErAs dot content at the interfaces, (1) no ErAs, (2) 8% areal coverage with dots, and (3) 25% areal coverage with dots; (B) a cross-sectional TEM of the SL with no ErAs dots at the interfaces, C) a high-resolution TEM of the ErAs dots; D) a cross-sectional and E) plan-view TEM of the sample with 8% of the interfaces covered with ErAs dots.

4.1.2 Time-domain thermoreflectance

Briefly, a high-energy (~100 mW) laser pulse impinges on a metal opto-thermal transducer layer on the sample, exciting surface electrons which quickly thermalize, sending a heat pulse propagating through the metal and then through the sample, away from the surface. A time-delayed probe pulse measures the changing surface reflectivity with changing temperature. A multi-dimensional, multi-layer heat equation is fit to the resulting cooling curve, yielding the thermal conductivity of the SL layers [98]. The system used herein is described in further detail in Chapter 1 of this thesis and in a previous publication [68]. We deposited a 100 nm Al optothermal transducer layer on the SLs and a calibration sapphire substrate. We confirmed the thickness of the Al transducer layer by matching the TDTR-measured thermal conductivity value of the sapphire substrate with the known literature value. Low-temperature measurements were conducted by mounting the samples in a low-vacuum ($\sim 10^{-6}$ torr) cryostat. The temperature of the surface of the samples was measured with a Si diode.

Each sample was probed at between three or five different locations. At each location, the samples were measured under four different pump modulation frequencies - 3, 6, 9, and 12 MHz, with three individual data traces collected for each modulation frequency. The three runs at each frequency were averaged, and the Fourier fitting analysis was performed on the resultant average curve at each modulation frequency for each location. Error bars represent the standard deviation from the results of these fittings.

The data were fit to a four-layer model comprising the metal optothermal transducer, the interface between the metal and the SL, the SL, and a semi-infinite substrate. The data were fit for the interface conductance between the metal and the SL, and the SL thermal conductivity. The other required parameters for the fitting were taken from the literature. Since the volumetric fraction of ErAs is small compared to that of GaAs and AlAs (0.32 ML and 1 ML of ErAs per 10 ML of GaAs or AlAs for the 8% and 25% nanodot areal coverage samples, respectively), the heat capacity was taken to be the average of GaAs and AlAs. An initial guess for the interface conductance between the SL, capped by a 3 nm GaAs layer, and the Al optothermal transducer layer were taken from previous measurements of the interface conductance between a GaAs substrate and an Al layer deposited with an identical procedure. Sample data and fittings are given for the reference samples (in Fig. 4-2) and the samples with maximal ErAs coverage (Fig. 4-3).

4.2 Results

The overall trend of an increasing thermal conductivity with increasing sample length or number of periods was observed, matching previously reported trends which highlighted the role of coherent phonon heat conduction in the SLs [98]. This trend is shown in Fig. 4-4.

The thermal conductivities of the SLs as a function of temperature, measured with time-domain thermoreflectance (TDTR) [68, 84, 85], are shown in Fig. 4-5. The measured thermal conductivities of the reference SL samples, which have no ErAs at the interfaces, closely match previously reported trends [98] as also shown in Chapter 3 of this thesis. For all the SLs, the thermal conductivity rapidly increases with temperature up to approximately 100 K, after which the thermal conductivity roughly plateaus. For short periods, thermal conductivity also increases with an increasing number of periods, indicating the presence of coherent phonon thermal transport.

The addition of ErAs nanodots decreases the overall thermal conductivity, with a greater coverage of ErAs, leading to a greater decrease in the overall thermal conductivity, as seen in the insets in Fig. 4-6. High-frequency phonons are scattered by interface roughness and atomistic mixing. The addition of ErAs dots has the effect of scattering phonons in the intermediate-frequency range. As more dots are added, this range grows [25]. This is indicated by the decreasing thermal conductivity with increasing ErAs content and also, notably, by the greater overall decrease in thermal conductivity for the samples with more SL periods (Fig. 4-6), as compared to those

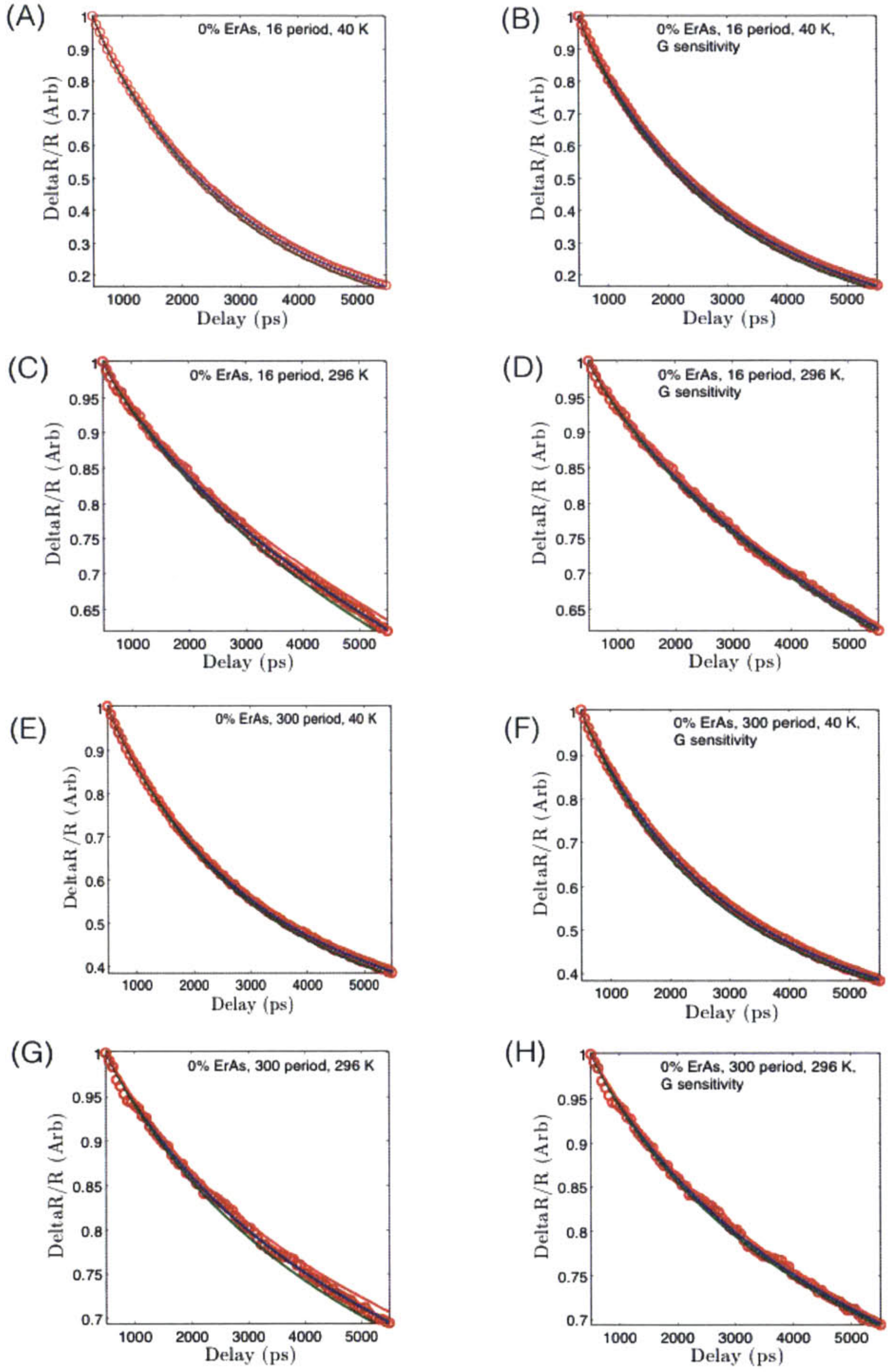

Figure 4-2: Representative data (open red circles) sets for (A)-(D) 16 period and (E)-(H) 300 period samples with no ErAs coverage at (A), (B), (E), and (F) 40 K and (C), (D), (G), and (H) 296 K showing the sensitivities to the fitting to both the (A), (C), (E), and (G) thermal conductivity measurements of the SLs and (B), (D), (F), and (H) the interface conductance measurement between the Al and the SL with +/- 10% lines for the best fit in red and green.

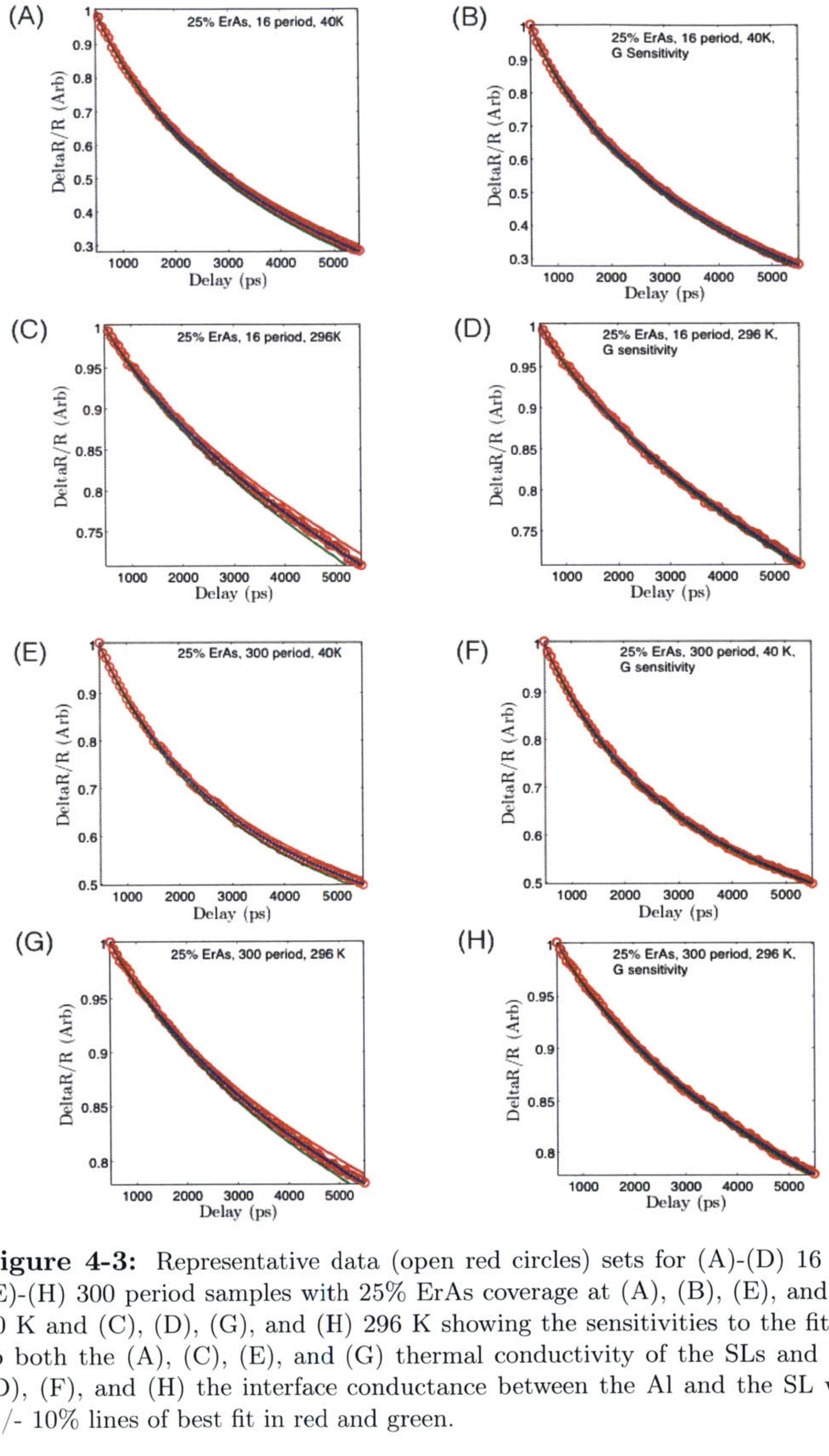

Figure 4-3: Representative data (open red circles) sets for (A)-(D) 16 and (E)-(H) 300 period samples with 25% ErAs coverage at (A), (B), (E), and (F) 40 K and (C), (D), (G), and (H) 296 K showing the sensitivities to the fitting to both the (A), (C), (E), and (G) thermal conductivity of the SLs and (B), (D), (F), and (H) the interface conductance between the Al and the SL with +/- 10% lines of best fit in red and green.

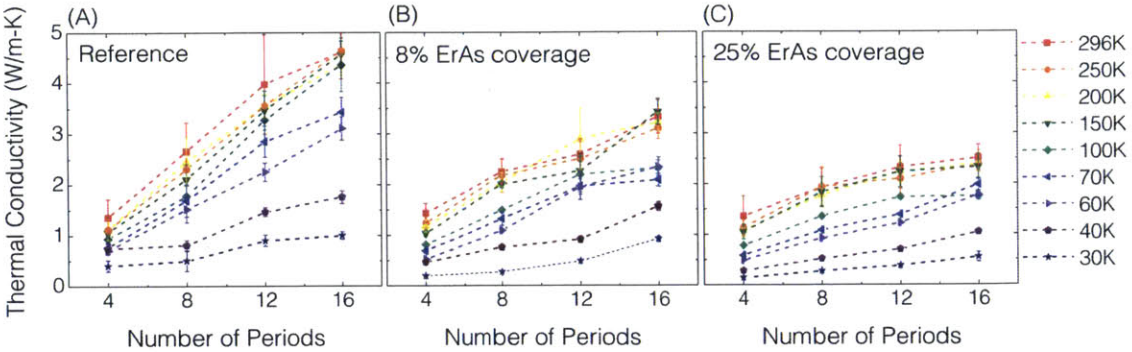

Figure 4-4: SL thermal conductivities for short period SLs as a function of the number of periods and at different temperatures for (A) reference GaAs/AlAs SLs with no ErAs nanodots, (B) GaAs/AlAs SLs with 8% areal coverage with ErAs nanodots, and (C) GaAs/AlAs SLs with 25% areal coverage with ErAs nanodots.

with a small number of periods because in the shorter SLs, the boundary between the SL and the substrate plays a similar role in reducing the effective mean free path. This latter effect bolsters the results of our previous work on coherent phonon heat conduction in SLs [98]. By adding scatterers at the SL interfaces, we are able to reduce the role of coherent phonon transport in SLs and decrease the SL bulk thermal conductivity by a factor of two. We should mention that the use of nanodots to increase scattering of intermediate wavelength phonons has been studied before both theoretically and experimentally [25, 140, 155, 156, 157]. In particular, Pernot *et al.* compared the measure thermal conductivities of Ge-dot based Si/Ge SLs with the thermal conductivity determined by Green's functions for Si/Ge SLs with perfect interfaces. This comparison showed that the Ge-dots based SLs can have 5x lower thermal conductivity than SLs without nanodots. The major differences between our study from this and other previous studies are that (1) GaAs/AlAs SLs with and without ErAs dots have identical crystal structures, allowing for a direct comparison of experimental data, and (2) whereas previous studies focused on thermally thick

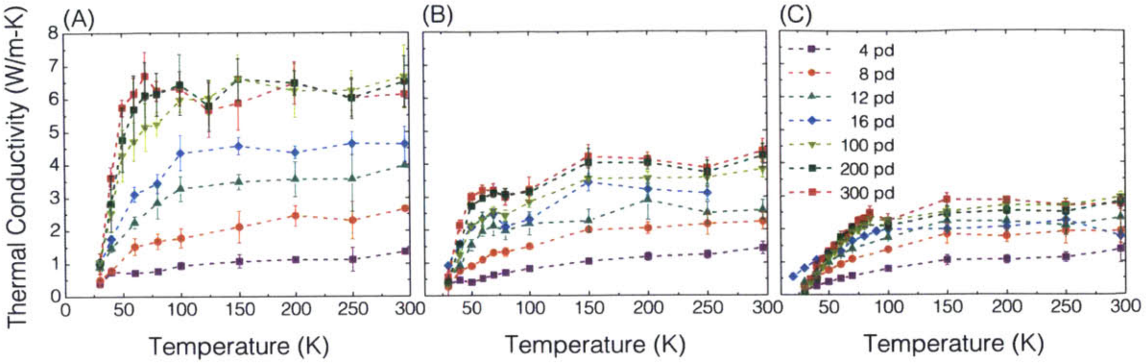

Figure 4-5: Thermal conductivity as a function of temperature for the temperature range 30 K - 296 K for the three sets of samples: (A) the reference samples, which have no ErAs at the interfaces, (B) the samples where 8% of the interfaces are covered in ErAs dots, and (C) the samples where 25% of the interfaces are covered with ErAs dots.

SLs with different period thicknesses, we fixed the thickness of the SL periods while varying the total thickness of the SLs. Our approach allows us to discover unique wave effects as we discuss below.

4.2.1 Raman measurements

We conducted a Raman scattering experiment to probe the first few bands of the folded band structure in the SLs since these phonons are the major contributors to heat conduction, especially at low temperatures. Raman experiments were performed by Shengxi Huang of Millie Desselhaus' group at MIT. The low-frequency (<100 cm-1) Raman spectra were obtained with a Horiba Jobin-Yvon T64000 triple-grating Raman spectrometer under a $Z(XX)\bar{Z}$ back-scattering configuration. The excitation laser was a frequency-doubled Nd:YAG laser with a wavelength of 532.5 nm, and the power incident on the sample was 7.2 mW. The measurement accumulation time was 60 seconds to ensure a sufficient signal-to-noise ratio. A 100X objective lens

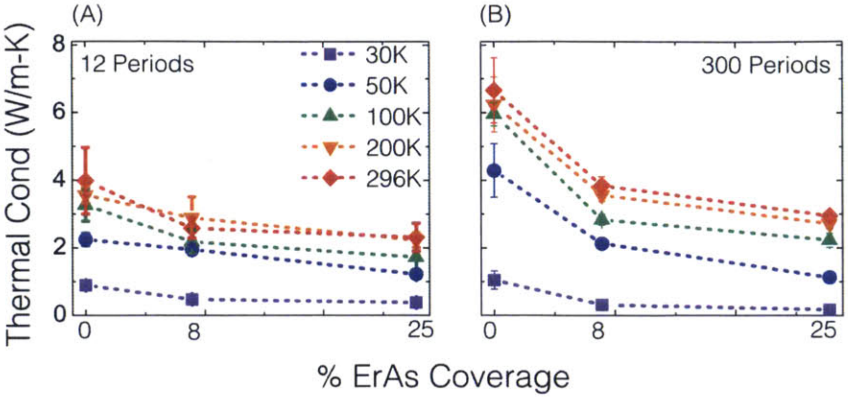

Figure 4-6: Thermal conductivity as a function of ErAs coverage for samples with 12 periods and samples with 300 periods.

with a numerical aperture (NA) of 0.95, a micrometer resolved XYZ motorized stage, and an 1800 lines/mm grating were used. Both Stokes and anti-Stokes lines were collected and were used for calibration of the instrument. In contrast to the low-frequency measurement, high-frequency (>100 cm^{-1}) spectra were measured with a Horiba Jobin-Yvon HR800 Raman spectrometer using an objective lens with an NA of 0.90, an incident excitation laser power on the sample of 1.2 mW, and a shorter accumulation time of 15 seconds. The other measurement configurations were the same.

Figure 4-7 shows the measured phonon spectra of the first two bands of selected SLs. The experiment measures transverse phonons at the zone center rather than the band edge [117], corresponding to the 2nd and 4th minibands in the extended zone representation. While the reference SLs show both the 2nd and 4th bands, the ErAs covered SLs do not display strong signals at the second bands. For 25% ErAs coverage, the first band disappears in the 300 period SL. We interpret the disappearing bands as a result of wave cancellation that leads to localization.

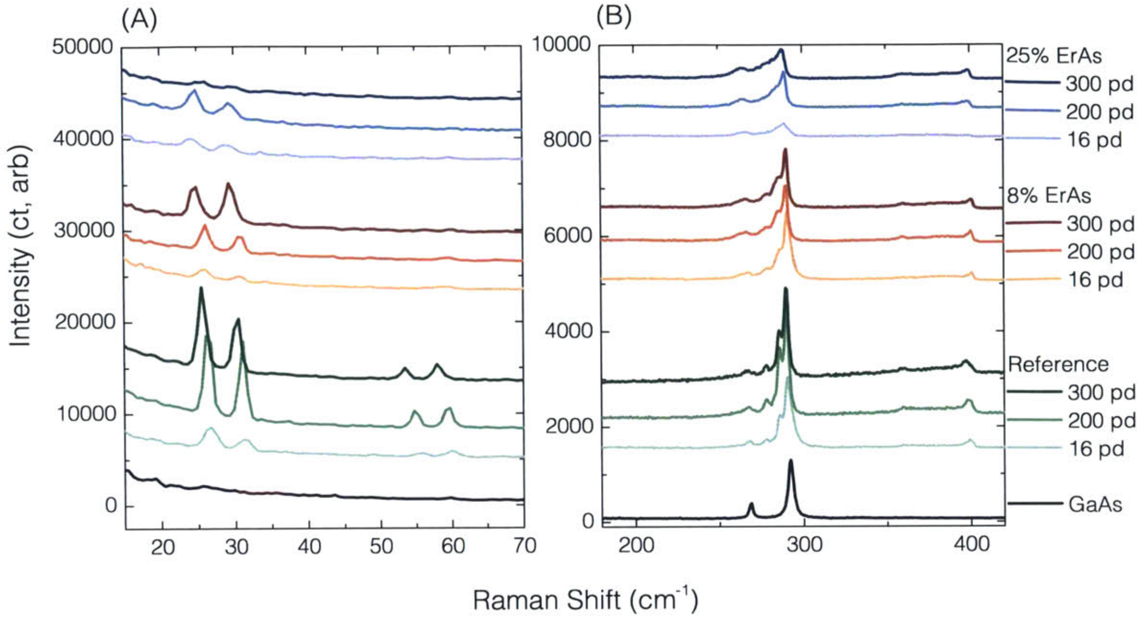

Figure 4-7: Raman spectra for representative SLs (16, 200, and 300 pd SLs with each level of ErAs coverage) in both the low-frequency (15-70 cm^{-1}) and high-frequency regimes (200-400 cm^{-1}).

4.3 Observations of Phonon Localization

The dependence of the thermal conductivity on the total length of the SLs reveals a very interesting trend. At temperatures above 100 K, the samples with a small number of periods (4, 8, 12, and 16 periods) uniformly show an increasing thermal conductivity with an increasing number of periods. The thermal conductivities of the SLs eventually saturates to a value that is much lower than either bulk parent material (45 W/m-K for GaAs and 90 W/m-K for AlAs [110]) and, in fact, the saturation value is lower than that of a corresponding bulk homogenous alloy (10 W/m-K [67]). This dependence is consistent with our previous report [98], confirming that some special phonons have MFPs longer than the total SL thickness. Simulations showed that these special phonons are long wavelength phonons which experience boundary scattering, as opposed to short wavelength phonons which are scattered by interface roughness.

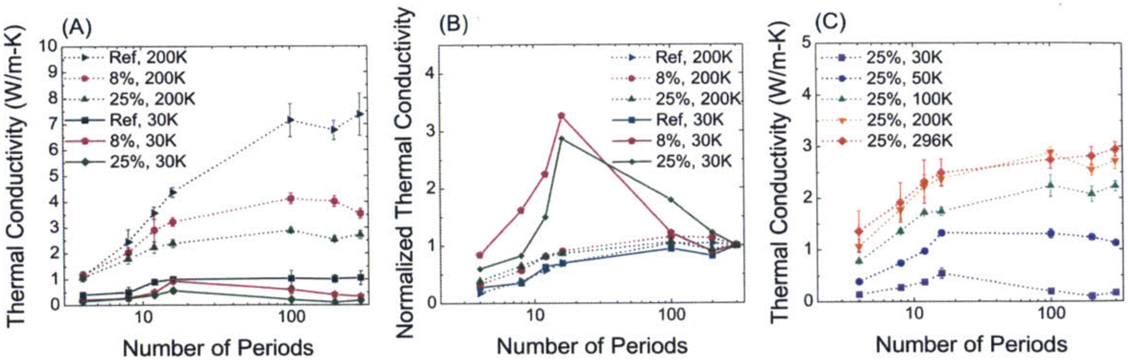

Figure 4-8: Thermal conductivity as a function of number of superlattice periods. (A) At 200 K, the thermal conductivity first increases with the number of periods and then saturates, suggesting that some phonon tranverse the SLs coherently. At 30 K, the thermal conductivity behaves similarly in the reference sample, but in the samples with many ErAs dots at the interfaces, the thermal conductivity decreases after reaching a peak at a small number (~16) of periods. When the thermal conductivities in (A) are normalized to the thermal conductivity of the longest sample as is done in (B), the anomalous low-temperature trend for samples with ErAs dots is even more pronounced. (C) As the temperature is increased, the thermal conductivity of the samples with 25% ErAs dots begins to match the trend seen in the reference sample, a uniform increase of the thermal conductivity with increasing number of periods.

At lower temperatures, SLs having a high concentration of ErAs (25%) show a different and surprising trend. Below 60 K, the SLs with 25% ErAs coverage and fewer periods (12 and 16 periods) have a higher thermal conductivity than the longest SLs, as seen in Fig. 4-8(A). The transition also happens to the 8% ErAs sample, but is absent from the referent samples. To show this more clearly, we normalize the measured thermal conductivities for all SL periods to the 300 period SL value for each sample. The resulting normalized thermal conductivity is shown in Fig. 4-8(B). This trend suggests that a means of reducing the transport of long-wavelength, low-frequency phonons is unfolding with an increasing sample length. Namely, the opposite of the effect of boundary scattering which reduces the transport of these phonons inversely with the sample size is seen. This unexpected trend strongly points to the presence of phonon localization in these samples. Localization effects in phonon transport are expected to unfold over an increasing distance, as certain phonon modes make the transition from being propagating to non-propagating modes [158, 159]. Thus, in samples where the localization length has been surpassed, the thermal conductivity is expected to be lower than in samples that are shorter than the localization length. This effect is emphasized in Fig. 4-8.

The localization of waves in general has been studied extensively [159, 160, 161]. Due to its broadband nature, however, the localization of heat conduction, like other wave effects, has proven experimentally elusive [162] until recently. A minimum in the thermal conductivity of some SLs was used by Venkatasubramanian as a sign of localization [163], but later works show it is the result of the competition between coherent and incoherent transport in SLs [58, 152]. The plateaus in the thermal conductivities of glasses and aggregates at low temperatures was thought of as a combined effect of localization and diffusion [164, 165, 166]. In these materials, however, MFPs are on the order of tens of angstroms, much shorter than in typical crystalline materials. A few publications have shown results of simulations, including molecular-dynamics simulations in SLs, with randomized period thicknesses [151] and continuum-mechanics based simulations of cross-section modulated core-shell nanowires superlattices [150]. These simulations are closer to low-dimensional structures, for which localization is easier to observe. Our experimental results suggest that localization of some phonon contributions to heat conduction in 3D, similar to the strong photon localization at the band edges in SLs with lateral disorder, as discussed by John [161].

Detecting phonon localization in thermal transport measurements has been exceedingly difficult due to the stringent criteria that localized phonons must meet. First, phonon localization is expected to occur at band edges due to the rapid reduction of the density of states and available phase space to scatter into [159]. Second, phonons contributing to thermal conduction span a wide range of frequencies. In bulk crystals where phonon transport dominates heat conduction, the wave vectors, k, at the band edges are high. In accordance with the modified Ioffe-Regel condition for strong wave localization in three dimensions, l x $k \leq 1$ [167], localized phonons in a bulk material have MFPs, l, on the order of angstroms. Since phonons contributing to the thermal conductivity in bulk crystals have much longer MFPs, observations of localization have been elusive in such 3D systems.

We can observe phonon localization contribution to the ErAs-dots doped GaAs/AlAs SLs because of several factors. First, natural interface mixing in GaAs/AlAs SLs scatters high-frequency phonons. According to DFT and atomic Green's function simulations, only low-frequency and long-wavelength phonons contribute to heat conduction in SLs [98, 168]. Second, zone folding in SLs reduces the wavevector at the BZ boundary by approximately an order of magnitude, from the lattice constant of bulk crystals (~5 Å) to the 6 nm lattice constant of the superlattice. The reduced wavevector allows longer MFP phonons to satisfy the Ioffe-Regel conduction. Third, the diameter of the ErAs is approximately 3 nm, and on average their spacing are 9 nm for the SLs with 8% coverage and 5 nm for the SLs with 25% areal coverage. These are comparable to the phonon wavelengths at the boundaries of the folded zone, increasing the multiple scatterings of these phonons, leading to their localization. At room temperature, contributions to the thermal conductivity comes from a broader range of phonons, while at lower temperatures, the populations shifts to lower frequency phonons, making the contributions from localized phonons observable.

The pump modulation frequency dependence of the thermal conductivity provides further evidence of the significant MFP reduction in SLs with ErAs nanodots. While k decreases with increasing modulation frequency in the 300 period reference SLs, as seen in Fig. 4-9(A), no such dependence exists in the 300 period SL with 25% interface coverage with ErAs dots (Fig. 4-9(B)). The modulation frequency dependence in the reference samples is indicative of ballistic transport. A lower modulation frequency leads to a deeper penetration of the thermal signal so that the resulting thermal conductivity has fewer trace ballistic effects [169]. In the reference samples, these trace ballistic effects, which effect long-wavelength phonons, are evident in the decreasing thermal conductivity with decreasing thermal penetration depth, or increasing pump modulation frequency [170]. The absence of these effects in the 300 period SL with 25% ErAs interface coverage, however, indicates that the long MFP phonons contributing to heat conduction in GaAs/AlAs SLs are reduced to nonobservable in the SLs with ErAs dots. Although this observation alone does not prove the presence of these localization effects, it is consistent with the consequences of localization.

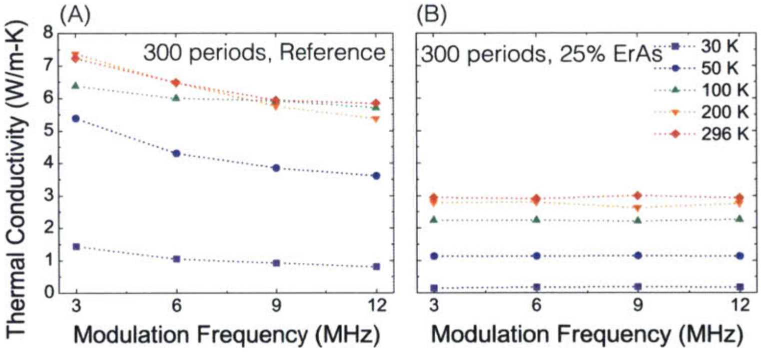

Figure 4-9: Thermal conductivity as a function of pump modulation frequency at a range of temperatures for the samples with no ErAs at the interfaces (red background) and the samples with 25% of the interfaces covered with ErAs nanodots. There is a clear trend of decreasing thermal conductivity with increasing modulation frequency in the samples with no ErAs, whereas there is no modulation frequency dependence of thermal conductivity in the samples with 25% ErAs coverage.

4.4 Summary

In summary, we have demonstrated the potential of engineering phonon waves to reduce thermal conductivity in SLs. By using ErAs nanodots, we reduce thermal conductivity of thick SLs by a factor a two compared to samples without dots. Furthermore, we provide evidence of phonon localization in ErAs nanodot-doped SLs at low temperatures. These observations open up new opportunities to engineer phonon thermal conductivity via wave effects.

Chapter 5

Summary and Outlook

5.1 Summary

The growing need for improving thermal designs for various applications, including the electronic, photonic, and energy harvesting industries has motivated research into attaining a better understanding of nanoscale thermal transport [17, 18]. A wide variety of nanostructures have been studied with a number of experimental and computational techniques in an effort to tease out a deeper understanding of the different thermal transport regimes of heat conduction. Superlattices (SLs) have played an especially large part of the study of thermal conduction at these small scales because of the relative ease of fabrication of SLs and the relative ease of simulating phonon-related phenomena in these SLs [27, 54, 60, 98, 171].

In this thesis, we explored various thermal transport phenomena in GaAs/AlAs SLs. In Chapter 2, we studied anisotropic thermal transport through these systems. This was the first observation of thermal conduction in both the in-plane and through-plane directions of the same samples [171]. The through-plane measurements are done with the time-domain thermoreflecance (TDTR) technique while the in-plane measurements are conducted with the transient thermal grating (TTG) technique. Both of these methods are non-contact optical pump-and-probe methods wherein a laser pulse excites a thermal response and the thermal response is measured in time. Working in tandem, it is possible to determine the thermal conductivity in both transport directions. These measurements add important data points to the growing data set of thermal transport through a variety of SL material systems and geometries. In addition, the results of the measurements can be compared to first-principles and DFT simulations of the system, enhancing the validity of these simulations for modeling these systems.

In Chapter 3, we approach the problem of observing coherent phonon transport through SLs with a new experimental paradigm. Rather than taking the traditional route of measuring the thermal conductivity through SLs with different period thicknesses but with constant total sample thicknesses, we used TDTR to measure thermal transport through SLs with a constant period thickness but a changing number of periods [98]. This technique combines the elements of SLs with thin films. It has been demonstrated through a variety of methods that in crystalline thin films, the thermal conductivity increases monotonically with sample size. This length-dependent thermal conductivity has been attributed to the Casimir picture, wherein phonons with mean free paths longer than the total sample thickness traverse the internal region of the thin film ballistically, scattering at the sample boundary. Previous experiments in SLs were unable to show this ballistic internal SL transport and thus thermal conduction was dominated by incoherent scattering at the internal interfaces at the SL. Observations of a monotonic increase of the thermal conductivity with total SL size shows that ballistic transport of long MFP phonons is occurring in these nanostructures, proving the presence of coherent phonon transport and the consequent buildup of an SL dispersion relation. The results of the experiments were corroborated by first-principles and Green's functions simulations. This was the first demonstration of coherent phonon thermal transport in SLs.

This experiment logically gave way to an experiment which attempted to break the residual phonon coherence. In the previous set of SLs, the overall reduction of the SL thermal conductivity compared to either bulk parent material is attributable to short-wavelength phonons scattering diffusively at the internal interfaces of the SL [98]. The residual thermal transport is due to long-wavelength phonons that traverse the inner region of the SL without scattering at the interfaces. GaAs/AlAs SLs with different areal coverages of ErAs nanodots at the internal interfaces were fabricated. TDTR measurements showed that these samples also exhibited coherent phonon heat conduction. In addition, the addition of the ErAs nanodots further decreased the overall thermal conductivity, with a greater concentration of ErAs nanodots correlating with a greater decrease in the thermal conductivity. This implies that the ErAs nanodots serve the same purpose for some longer-wavelength phonons as interface roughness serves for shorter-wavelength phonons, by scattering these phonons diffusively and preventing their contributions to thermal conduction.

Experiments at different temperatures also gave further insight into another interesting thermal phenomenon taking place in these SLs with interfacial nanodots. At the lowest temperatures, the SLs with a smaller number of periods had a thermal conductivity that exceeded the thermal conductivity of samples with larger numbers of periods. This points to the presence of localization effects in these SLs. Thus, with this new experimental paradigm, we have observed two wave regimes of phonon transport through SLs.

5.2 Outlook and Conclusion

This thesis explored the topic of thermal transport through SLs at great depth. The material system we studied was GaAs/AlAs superlattices. These two materials are relatively easy to model and are well lattice matched, making them easier to fabricate than many other systems [172]. However, the experimental concepts herein can be readily applied to other material systems and doing so would greatly enhance the understanding of thermal transport concepts. For example, studying the anisotropy of Si/Ge SLs would not only further add insight to the understanding of heat conduction through these structures, but add to the ever-growing data set about these structures. Additionally, much computational data exists about the Si/Ge system [61, 65, 112, 168], which anisotropy experimental data would help support. The technique for measuring anisotropic thermal transport by using the TDTR and TTG techniques in tandem can also be applied more broadly to other nanostructures where anisotropic thermal transport is expected. For example, graphene based materials are currently of great interest and thermal transport through graphene is known to be anisotropic. The cross-plane thermal conductivity of disordered layered WSe2 was recently measured in the cross-plane direction, and determined to have an ultra-low thermal conductivity [146]. This system is expected to have highly anisotropic thermal transport which could be determined with the combination of the TDTR and TTG techniques. Similar opportunities await the study of coherent phonon heat conduction and localization. SLs are not the only systems where these effects could be found. The combination of a nanostructure and a thin film could be applied to other nanostructures, such as nanoporous Si.

Detecting coherent phonon heat transport in superlattices opens new venues for the possible manipulation and control of phonon transport through the design of materials with favorable phonon wave properties. Adding ErAs nanodots to the GaAs/AlAs SL system was effective in further reducing the thermal conductivity of these nanostructures because it created longer-range structural perturbations than interface roughness. Other ways to achieve a similar reduction include adding strain or aperiodicity to the system. These effects might similarly reduce the overall thermal conductivities in GaAs/AlAs SLs. Adding the ErAs nanodots created an interesting effect at low temperatures. The thermal conductivities of the shorter SLs were higher than that of the longer SLs. This unexpected dependence on the length of the SLis attributed to phonon localization, an effect that builds over multiple periods and affects mid-range phonons. More sophisticated simulations need to be performed in order to confirm the origins of this thermal conductivity trend. Further experiments on SLs with long-range perturbations, such as strain and long-range aperiodicity, should also be explored with a similar thin-film paradigm to see whether these localization effects are still present. The experimental results could help guide computational efforts to understand phonon localization and coherent phonon heat conduction.

Finally, the intent of many of the experiments conducted herein was to observe the signatures of previously unobserved thermal transport regimes. The TDTR system provides a powerful technique for examining thermal transport at such small scales, but the interpretation of the data has lagged behind the physical understanding of these processes. Specifically, the data, which are used to show the breakdown of Fourier's law at these small scales, are interpreted with a Fourier's law analysis. While this is sufficient for recognizing a trend and for determining an effective thermal conductivity through the studied nanostructures, it is likely masking important details of the thermal conductivity [173, 174]. Furthermore, matching simulation results to experimental results exactly is difficult when simulation techniques have become much more sophisticated than data analysis techniques. The realization of impressive fabrication, experimentation, and simulation techniques that are now available calls for an update to the data interpretation from these experiments.

Bibliography

[1] A. Fick, "V. On liquid diffusion," *The London, Edinburgh, and Dublin Philosophical Magazine and Journal of Science*, vol. 10, no. 63, pp. 30–39, 1855.

[2] J. van't Hoff, "The function of osmotic pressure in the analogy between solutions and gases," *Proceedings of the Physical Society of London*, vol. 9, no. 1, p. 307, 1887.

[3] E. Buckingham, "Studies on the movement of soil moisture," 1907.

[4] L. A. Richards, "Capillary conduction of liquids through porous mediums," *Journal of Applied Physics*, vol. 1, no. 5, pp. 318–333, 1931.

[5] L. Rayleigh, *The Theory of Sounds, 2nd.* 1894.

[6] A. Einstein, "On the electrodynamics of moving bodies," *Annalen der Physik*, vol. 17, no. 10, pp. 891–921, 1905.

[7] W. C. Roberts-Austen, "Bakerian Lecture: On the diffusion of metals," *Philosophical Transactions of the Royal Society of London. Series A, Containing Papers of a Mathematical or Physical Character*, pp. 383–415, 1896.

[8] F. Y. Edgeworth, "XLII. The law of error," *The London, Edinburgh, and Dublin Philosophical Magazine and Journal of Science*, vol. 16, no. 100, pp. 300–309, 1883.

[9] G. S. Ohm, *The Galvonic current investigated mathematically.* 1827.

[10] W. Thomson, "On the univorm motion of heat in homogeneous solid bodies and its connection with the mathematical theory of electricity.," *Cambridge mathematical journal*, vol. 3, pp. 71–84, 1842.

[11] E. Amaldi and E. Fermi, "On the absorption and the diffusion of slow neutrons.," *Physical Review*, vol. 50, no. 10, p. 899, 1936.

[12] W. de Haas and T. Biermasz, "The thermal conductivity of diamond and potassium chloride," *Physica*, vol. 5, pp. 47–53, Jan. 1938.

[13] W. de Haas and T. Biermasz, "The dependence on thickness of the thermal resistance of crystals at low temperatures," *Physica*, vol. 5, pp. 619–624, July 1938.

[14] R. Peierls, "Zur kinetischen Theorie der Wärmeleitung in Kristallen," *Annalen der Physik*, vol. 395, no. 8, pp. 1055–1101, 1929.

[15] H. B. G. Casimir, "Note on the conduction of heat in crystals," *Physica*, vol. 5, no. 6, pp. 495–500, 1938.

[16] L. Page, "Review: J. Frenkel, Wave Mechanics. Elementary Theory," *Bulletin of the American Mathematical Society*, vol. 39, p. 494, July 1933.

[17] D. G. Cahill, W. K. Ford, K. E. Goodson, G. D. Mahan, A. Majumdar, H. J. Maris, R. Merlin, and S. R. Phillpot, "Nanoscale thermal transport," *Journal of Applied Physics*, vol. 93, no. 2, p. 793, 2003.

[18] D. G. Cahill, P. V. Braun, G. Chen, D. R. Clarke, S. Fan, K. E. Goodson, P. Keblinski, W. P. King, G. D. Mahan, A. Majumdar, H. J. Maris, S. R. Phillpot, E. Pop, and L. Shi, "Nanoscale thermal transport. II. 2003-2012," Jan. 2014.

[19] K. Zhang, U. Bhattacharya, Z. Chen, F. Hamzaoglu, D. Murray, N. Vallepalli, Y. Wang, B. Zheng, and M. Bohr, "A 3-GHz 70-Mb SRAM in 65-nm CMOS

Technology With Integrated Column-Based Dynamic Power Supply," *IEEE Journal of Solid-State Circuits*, vol. 41, pp. 146–151, Jan. 2006.

[20] C. Auth, C. Allen, A. Blattner, D. Bergstrom, M. Brazier, M. Bost, M. Buehler, V. Chikarmane, T. Ghani, T. Glassman, R. Grover, W. Han, D. Hanken, M. Hattendorf, P. Hentges, R. Heussner, J. Hicks, D. Ingerly, P. Jain, S. Jaloviar, R. James, D. Jones, J. Jopling, S. Joshi, C. Kenyon, H. Liu, R. McFadden, B. McIntyre, J. Neirynck, C. Parker, L. Pipes, I. Post, S. Pradhan, M. Prince, S. Ramey, T. Reynolds, J. Roesler, J. Sandford, J. Seiple, P. Smith, C. Thomas, D. Towner, T. Troeger, C. Weber, P. Yashar, K. Zawadzki, and K. Mistry, "A 22nm high performance and low-power CMOS technology featuring fully-depleted tri-gate transistors, self-aligned contacts and high density MIM capacitors," in *2012 Symposium on VLSI Technology (VLSIT)*, pp. 131–132, IEEE, June 2012.

[21] M. Ieong, B. Doris, J. Kedzierski, K. Rim, and M. Yang, "Silicon device scaling to the sub-10-nm regime.," *Science (New York, N.Y.)*, vol. 306, pp. 2057–60, Dec. 2004.

[22] A. D. Franklin, M. Luisier, S.-J. Han, G. Tulevski, C. M. Breslin, L. Gignac, M. S. Lundstrom, and W. Haensch, "Sub-10 nm carbon nanotube transistor.," *Nano Letters*, vol. 12, pp. 758–62, Feb. 2012.

[23] C. Mack, "The Multiple Lives of Moore's Law," *IEEE Spectrum*, vol. 52, pp. 31–31, Apr. 2015.

[24] H. Esmaeilzadeh, E. Blem, R. St.Amant, K. Sankaralingam, and D. Burger, "Dark silicon and the end of multicore scaling," 2011.

[25] W. Kim, J. Zide, A. Gossard, D. Klenov, S. Stemmer, A. Shakouri, and A. Majumdar, "Thermal Conductivity Reduction and Thermoelectric Figure of Merit Increase by Embedding Nanoparticles in Crystalline Semiconductors," *Physical Review Letters*, vol. 96, p. 045901, Feb. 2006.

[26] B. Poudel, Q. Hao, Y. Ma, Y. Lan, A. Minnich, B. Yu, X. Yan, D. Wang, A. Muto, D. Vashaee, X. Chen, J. Liu, M. S. Dresselhaus, G. Chen, and Z. Ren, "High-thermoelectric performance of nanostructured bismuth antimony telluride bulk alloys.," *Science (New York, N.Y.)*, vol. 320, pp. 634–8, May 2008.

[27] W. Capinski and H. Maris, "Thermal conductivity of GaAs/AlAs superlattices," *Physica B: Condensed Matter*, vol. 219-220, pp. 699–701, Apr. 1996.

[28] S. M. Lee, D. G. Cahill, and R. Venkatasubramanian, "Thermal conductivity of SiGe superlattices," *Applied Physics Letters*, vol. 70, no. 22, p. 2957, 1997.

[29] P. Kim, L. Shi, A. Majumdar, and P. McEuen, "Thermal Transport Measurements of Individual Multiwalled Nanotubes," *Physical Review Letters*, vol. 87, p. 215502, Oct. 2001.

[30] D. Li, Y. Wu, P. Kim, L. Shi, P. Yang, and A. Majumdar, "Thermal conductivity of individual silicon nanowires," *Applied Physics Letters*, vol. 83, p. 2934, Sept. 2003.

[31] J.-K. Yu, S. Mitrovic, D. Tham, J. Varghese, and J. R. Heath, "Reduction of thermal conductivity in phononic nanomesh structures," *Nature Nanotechnology*, vol. 5, pp. 718–721, Oct. 2010.

[32] A. Ward, D. A. Broido, D. A. Stewart, and G. Deinzer, "Ab initio theory of the lattice thermal conductivity in diamond," *Physical Review B*, vol. 80, p. 125203, Sept. 2009.

[33] K. Esfarjani, J. Garg, and G. Chen, "Modeling Heat Conduction from First Principles," *Annual Review of Heat Transfer*, pp. 9–47, 2014.

[34] P. Giannozzi, S. de Gironcoli, P. Pavone, and S. Baroni, "Ab initio calculation of phonon dispersions in semiconductors," *Physical Review B*, vol. 43, pp. 7231–7242, Mar. 1991.

[35] P. Giannozzi, S. Baroni, N. Bonini, M. Calandra, R. Car, C. Cavazzoni, D. Ceresoli, G. L. Chiarotti, M. Cococcioni, I. Dabo, a. D. Corso, S. Fabris, G. Fratesi, S. De Gironcoli, R. Gebauer, U. Gerstmann, C. Gougoussis, A. Kokalj, M. Lazzeri, L. Martin-Samos, N. Marzari, F. Mauri, R. Mazzarello, S. Paolini, A. Pasquarello, L. Paulatto, C. Sbraccia, S. Scandolo, G. Sclauzero, a. P. Seitsonen, A. Smogunov, P. Umari, and R. M. Wentzcovitch, "Quantum ESPRESSO: a modular and open-source software project for quantum simulations of materials," *Journal of Physics: Condensed Matter*, vol. 21, p. 36, Sept. 2009.

[36] E. N. Economou, *Green's functions in quantum physics.* New York: Springer, 1984.

[37] N. Mingo and L. Yang, "Phonon transport in nanowires coated with an amorphous material: An atomistic Green'Źs function approach," *Physical Review B*, vol. 68, p. 245406, Dec. 2003.

[38] F. Müller-Plathe, "A simple nonequilibrium molecular dynamics method for calculating the thermal conductivity," *The Journal of Chemical Physics*, vol. 106, p. 6082, Apr. 1997.

[39] J. Howell, "The monte carlo method in radiative heat transfer," *Journal of Heat Transfer*, vol. 120, no. 3, pp. 547–560, 1998.

[40] M.-S. Jeng, R. Yang, D. Song, and G. Chen, "Modeling the Thermal Conductivity and Phonon Transport in Nanoparticle Composites Using Monte Carlo Simulation," *Journal of Heat Transfer*, vol. 130, p. 042410, Apr. 2008.

[41] T. Luo and G. Chen, "Nanoscale heat transfer - from computation to experiment.," *Physical chemistry chemical physics : PCCP*, vol. 15, pp. 3389–412, Feb. 2013.

[42] S. Lee, D. Broido, K. Esfarjani, and G. Chen, "Hydrodynamic phonon transport in suspended graphene.," *Nature communications*, vol. 6, p. 6290, Jan. 2015.

[43] A. Debernardi, S. Baroni, and E. Molinari, "Anharmonic Phonon Lifetimes in Semiconductors from Density-Functional Perturbation Theory," *Physical Review Letters*, vol. 75, pp. 1819–1822, Aug. 1995.

[44] D. A. Broido, M. Malorny, G. Birner, N. Mingo, and D. A. Stewart, "Intrinsic lattice thermal conductivity of semiconductors from first principles," *Applied Physics Letters*, vol. 91, no. 23, p. 231922, 2007.

[45] A. F. Ioffe, "On thermal conduction in semiconductors," *Il Nuovo Cimento*, vol. 3, pp. 702–715, Apr. 1956.

[46] K. Biswas, J. He, Q. Zhang, G. Wang, C. Uher, V. P. Dravid, and M. G. Kanatzidis, "Strained endotaxial nanostructures with high thermoelectric figure of merit.," *Nature chemistry*, vol. 3, pp. 160–6, Feb. 2011.

[47] K. Biswas, J. He, I. D. Blum, C.-I. Wu, T. P. Hogan, D. N. Seidman, V. P. Dravid, and M. G. Kanatzidis, "High-performance bulk thermoelectrics with all-scale hierarchical architectures.," *Nature*, vol. 489, pp. 414–8, Sept. 2012.

[48] E. T. Swartz and R. O. Pohl, "Thermal boundary resistance," *Reviews of Modern Physics*, vol. 61, pp. 605–668, July 1989.

[49] G. Chen, *Nanoscale energy transport and conversion: a parallel treatment of electrons, molecules, phonons, and photons.* Oxford University Press, USA, 2005.

[50] V. Narayanamurti, "Phonon optics and phonon propagation in semiconductors.," *Science (New York, N.Y.)*, vol. 213, pp. 717–723, Aug. 1981.

[51] J. P. W. S. Tamura, D. C. Hurley, "Acoustic-phonon propagation in superlattices," *Physical Review B*, vol. 38, no. 2, pp. 1427–1449, 1988.

[52] L. Esaki and R. Tsu, "Superlattice and Negative Differential Conductivity in Semiconductors," *IBM Journal of Research and Development*, vol. 14, pp. 61–65, Jan. 1970.

[53] X. Y. Yu, G. Chen, A. Verma, and J. S. Smith, "Temperature dependence of thermophysical properties of GaAs/AlAs periodic structure," *Applied Physics Letters*, vol. 67, p. 3554, Dec. 1995.

[54] W. S. Capinski, H. J. Maris, T. Ruf, M. Cardona, K. Ploog, and D. S. Katzer, "Thermal-conductivity measurements of GaAs/AlAs superlattices using a picosecond optical pump-and-probe technique," *Physical Review B*, vol. 59, no. 12, pp. 8105–8113, 1999.

[55] G. Chen, "Thermal conductivity and ballistic-phonon transport in the cross-plane direction of superlattices," *Physical Review B*, vol. 57, pp. 14958–14973, June 1998.

[56] Y. K. Koh, Y. Cao, D. G. Cahill, and D. Jena, "Heat-Transport Mechanisms in Superlattices," *Advanced Functional Materials*, vol. 19, pp. 610–615, Feb. 2009.

[57] A. S. Barker, J. L. Merz, and A. C. Gossard, "Study of zone-folding effects on phonons in alternating monolayers of GaAs-AlAs," *Physical Review B*, vol. 17, pp. 3181–3196, Apr. 1978.

[58] M. Simkin and G. Mahan, "Minimum thermal conductivity of superlattices," *Physical review letters*, vol. 84, pp. 927–30, Jan. 2000.

[59] V. Narayanamurti, H. L. Stomer, M. A. Chin, A. Gossard, and W. Wiegmann, "Selective Transmission of High-Frequency Phonons by a Sperlattice: The "Dielectric" Phonon Filter," *Physical Review Letters*, vol. 43, no. 27, pp. 2012–2016, 1979.

[60] S. T. Huxtable, A. R. Abramson, C.-L. Tien, A. Majumdar, C. LaBounty, X. Fan, G. Zeng, J. E. Bowers, A. Shakouri, and E. T. Croke, "Thermal conductivity of Si/SiGe and SiGe/SiGe superlattices," *Applied Physics Letters*, vol. 80, p. 1737, Mar. 2002.

[61] S.-i. Tamura, Y. Tanaka, and H. Maris, "Phonon group velocity and thermal conduction in superlattices," *Physical Review B*, vol. 60, no. 4, pp. 2627–2630, 1999.

[62] W. E. Bies, R. J. Radtke, and H. Ehrenreich, "Phonon dispersion effects and the thermal conductivity reduction in GaAs/AlAs superlattices," *Journal of Applied Physics*, vol. 88, p. 1498, Aug. 2000.

[63] B. Yang and G. Chen, "Partially coherent phonon heat conduction in superlattices," *Physical Review B*, vol. 67, p. 195311, May 2003.

[64] J. Garg, N. Bonini, and N. Marzari, "High thermal conductivity in short-period superlattices.," *Nano Letters*, vol. 11, no. 12, pp. 5135–41, 2011.

[65] P. Hyldgaard and G. D. Mahan, "Phonon superlattice transport," *Physical Review B*, vol. 56, no. 17, pp. 10754–10757, 1997.

[66] G. Chen, "Size and Interface Effects on Thermal Conductivity of Superlattices and Periodic Thin-Film Structures," *Journal of Heat Transfer*, vol. 119, no. 2, p. 220, 1997.

[67] T. Yao, "Thermal properties of AlAs/GaAs superlattices," *Applied Physics Letters*, vol. 51, no. 22, p. 1798, 1987.

[68] A. J. Schmidt, X. Chen, and G. Chen, "Pulse accumulation, radial heat conduction, and anisotropic thermal conductivity in pump-probe transient thermoreflectance.," *The Review of Scientific Instruments*, vol. 79, p. 114902, Nov. 2008.

[69] A. I. Boukai, Y. Bunimovich, J. Tahir-Kheli, J.-K. Yu, W. A. Goddard, and J. R. Heath, "Silicon nanowires as efficient thermoelectric materials.," *Nature*, vol. 451, pp. 168–71, Jan. 2008.

[70] A. I. Hochbaum, R. Chen, R. D. Delgado, W. Liang, E. C. Garnett, M. Najarian, A. Majumdar, and P. Yang, "Enhanced thermoelectric performance of rough silicon nanowires.," *Nature*, vol. 451, pp. 163–7, Jan. 2008.

[71] J. Lim, K. Hippalgaonkar, S. C. Andrews, A. Majumdar, and P. Yang, "Quantifying surface roughness effects on phonon transport in silicon nanowires.," *Nano Letters*, vol. 12, no. 5, pp. 2475–82, 2012.

[72] A. Mavrokefalos, A. L. Moore, M. T. Pettes, L. Shi, W. Wang, and X. Li, "Thermoelectric and structural characterizations of individual electrodeposited bismuth telluride nanowires," *Journal of Applied Physics*, vol. 105, p. 104318, May 2009.

[73] H. Kim, I. Kim, H.-j. Choi, and W. Kim, "Thermal conductivities of $\mathrm{Si}_{1-x}\mathrm{Ge}_x$ nanowires with different germanium concentrations and diameters," *Applied Physics Letters*, vol. 96, p. 233106, June 2010.

[74] A. L. Moore, M. T. Pettes, F. Zhou, and L. Shi, "Thermal conductivity suppression in bismuth nanowires," *Journal of Applied Physics*, vol. 106, p. 034310, Aug. 2009.

[75] Z. Wang and N. Mingo, "Diameter dependence of SiGe nanowire thermal conductivity," *Applied Physics Letters*, vol. 97, p. 101903, Sept. 2010.

[76] C. W. Chang, D. Okawa, A. Majumdar, and A. Zettl, "Solid-state thermal rectifier.," *Science (New York, N.Y.)*, vol. 314, pp. 1121–4, Nov. 2006.

[77] J. Tang, H.-T. Wang, D. H. Lee, M. Fardy, Z. Huo, T. P. Russell, and P. Yang, "Holey silicon as an efficient thermoelectric material.," *Nano Letters*, vol. 10, pp. 4279–83, Oct. 2010.

[78] J.-H. Lee, G. A. Galli, and J. C. Grossman, "Nanoporous Si as an efficient thermoelectric material.," *Nano Letters*, vol. 8, pp. 3750–4, Nov. 2008.

[79] J.-H. Lee, J. C. Grossman, J. Reed, and G. Galli, "Lattice thermal conductivity of nanoporous Si: Molecular dynamics study," *Applied Physics Letters*, vol. 91, p. 223110, Nov. 2007.

[80] Y. He, D. Donadio, J.-H. Lee, J. C. Grossman, and G. Galli, "Thermal transport in nanoporous silicon: interplay between disorder at mesoscopic and atomic scales.," *ACS nano*, vol. 5, pp. 1839–44, Mar. 2011.

[81] N. K. Ravichandran and A. J. Minnich, "Coherent and incoherent thermal transport in nanomeshes," *Physical Review B*, vol. 89, p. 205432, May 2014.

[82] Y. Imry and R. Landauer, "Conductance viewed as transmission," *Reviews of Modern Physics*, vol. 71, pp. S306–S312, Mar. 1999.

[83] C. A. Paddock and G. L. Eesley, "Transient thermoreflectance from thin metal films," *Journal of Applied Physics*, vol. 60, no. 1, p. 285, 1986.

[84] W. S. Capinski and H. J. Maris, "Improved apparatus for picosecond pump-and-probe optical measurements," *Review of Scientific Instruments*, vol. 67, no. 8, p. 2720, 1996.

[85] D. G. Cahill, "Analysis of heat flow in layered structures for time-domain thermoreflectance," *Review of Scientific Instruments*, vol. 75, p. 5119, Nov. 2004.

[86] H. Carslaw and J. Jaeger, *Conduction of Heat in Solids.* New York: Oxford University Press, 1959.

[87] I. Chowdhury, R. Prasher, K. Lofgreen, G. Chrysler, S. Narasimhan, R. Mahajan, D. Koester, R. Alley, and R. Venkatasubramanian, "On-chip cooling by superlattice-based thin-film thermoelectrics," *Nature Nanotechnology*, vol. 4, no. April, pp. 235–238, 2009.

[88] R. Venkatasubramanian, E. Siivola, T. Colpitts, and B. O'Quinn, "Thin-film thermoelectric devices with high room-temperature figures of merit.," *Nature*, vol. 413, pp. 597–602, Oct. 2001.

[89] J. Faist, F. Capasso, D. L. Sivco, C. Sirtori, A. L. Hutchinson, and A. Y. Cho, "Quantum Cascade Laser," *Science (New York, N.Y.)*, vol. 264, pp. 553–556, 1994.

[90] T. Borca-Tasciuc, W. Liu, J. Liu, T. Zeng, D. W. Song, C. D. Moore, G. Chen, K. L. Wang, M. S. Goorsky, T. Radetic, R. Gronsky, T. Koga, and M. S. Dresselhaus, "Thermal conductivity of symmetrically strained Si/Ge superlattices," *Superlattices and Microstructures*, vol. 28, pp. 199–206, Sept. 2000.

[91] W. L. Liu, T. Borca-Tasciuc, G. Chen, J. Liu, and K. Wang, "Anisotropic Thermal Conductivity of Ge Quantum-Dot and Symmetrically Strained Si/Ge Superlattices," *Journal of Nanoscience and Nanotechnology*, vol. 1, no. 1, pp. 39–42, 2001.

[92] T. Borca-Tasciuc, A. R. Kumar, and G. Chen, "Data reduction in 3ω method for thin-film thermal conductivity determination," *Review of Scientific Instruments*, vol. 72, no. 4, p. 2139, 2001.

[93] B. Yang, W. L. Liu, J. L. Liu, K. L. Wang, and G. Chen, "Measurements of anisotropic thermoelectric properties in superlattices," *Applied Physics Letters*, vol. 81, no. 19, p. 3588, 2002.

[94] D. G. Cahill, "Thermal conductivity measurement from 30 to 750 K: the 3ω method," *Review of Scientific Instruments*, vol. 61, no. 2, p. 802, 1990.

[95] G. Chen, C. L. Tien, X. Wu, and J. S. Smith, "Thermal Diffusivity Measurement of GaAs/AlGaAs Thin-Film Structures," *Journal of Heat Transfer*, vol. 116, no. 2, p. 325, 1994.

[96] B. Yang and G. Chen, "Experimental Studies on Thermal Conductivity of Thin Film and Superlattices," in *Thermal Conductivity: Theory, Properties, and Applications* (T. Tritt, ed.), ch. 1.7, pp. 167–182, New York: Kluwer Academic/Plenum Publishers, 2004.

[97] S. Volz, J. B. Saulnier, G. Chen, and P. Beauchamp, "Computation of thermal conductivity of Si/Ge superlattices by molecular dynamics techniques," *Microelectronics Journal*, vol. 31, no. 9-10, pp. 815–819, 2000.

[98] M. N. Luckyanova, J. Garg, K. Esfarjani, A. Jandl, M. T. Bulsara, A. J. Schmidt, A. J. Minnich, S. Chen, M. S. Dresselhaus, Z. Ren, E. A. Fitzgerald, and G. Chen, "Coherent phonon heat conduction in superlattices," *Science*, vol. 338, pp. 936–9, Nov. 2012.

[99] D. G. Cahill, K. Goodson, and A. Majumdar, "Thermometry and Thermal Transport in Micro/Nanoscale Solid-State Devices and Structures," *Journal of Heat Transfer*, vol. 124, no. 2, p. 223, 2002.

[100] J. A. Rogers, A. A. Maznev, M. J. Banet, and K. A. Nelson, "Optical generation and characterization of acoustic waves in thin films," *Annu. Rev. Mater. Sci.*, vol. 30, pp. 117–157, 2000.

[101] J. E. Graebner, "Measurement of thermal diffusivity by optical excitation and infrared detection of a transient thermal grating," *Review of Scientific Instruments*, vol. 66, no. 7, p. 3903, 1995.

[102] C. D. Marshall, A. Tokmakoff, I. M. Fishman, C. B. Eom, J. M. Phillips, and M. D. Fayer, "Thermal boundary resistance and diffusivity measurements on thin $YBa_2Cu_3O_7$ films with MgO and $SrTiO_3$ substrates using the transient grating method," *Journal of Applied Physics*, vol. 73, no. 2, p. 850, 1993.

[103] J. A. Johnson, A. A. Maznev, M. T. Bulsara, E. A. Fitzgerald, T. C. Harman, S. Calawa, C. J. Vineis, G. Turner, and K. A. Nelson, "Phase-controlled, heterodyne laser-induced transient grating measurements of thermal transport properties in opaque material," *Journal of Applied Physics*, vol. 111, no. 2, p. 023503, 2012.

[104] G. D. Goodno, G. Dadusc, and R. J. D. Miller, "Ultrafast heterodyne-detected transient-grating spectroscopy using diffractive optics," *J. Opt. Soc. Am. B*, vol. 15, no. 6, pp. 1791–1794, 1998.

[105] A. A. Maznev, K. A. Nelson, and J. A. Rogers, "Optical heterodyne detection of laser-induced gratings.," *Optics letters*, vol. 23, pp. 1319–21, Aug. 1998.

[106] O. Kading, H. Skurk, A. A. Maznev, and E. Matthias, "Transient thermal gratings at surfaces for thermal characterization of bulk materials and thin films," *Appl. Phys. A*, vol. 61, pp. 253–261, 1995.

[107] D. H. Hurley, O. B. Wright, O. Matsuda, and S. L. Shinde, "Time resolved imaging of carrier and thermal transport in silicon," *Journal of Applied Physics*, vol. 107, no. 2, p. 023521, 2010.

[108] B. A. Ruzicka, L. K. Werake, H. Samassekou, and H. Zhao, "Ambipolar diffusion of photoexcited carriers in bulk GaAs," *Applied Physics Letters*, vol. 97, no. 26, p. 262119, 2010.

[109] H. Hillmer, A. Forchel, and C. W. Tu, "Enhancement of electron-hole pair mobilities in thing GaAs/$Al_xGa_{1-x}As$ quantum wells," *Physical Review B*, vol. 45, no. 3, pp. 1240–1245, 1992.

[110] S. Adachi, *GaAs and Related Materials: Bulk Semiconducting and Superlattice Properties.* River Edge, NJ: World Scientific, 1994.

[111] J. Garg and G. Chen, "Minimum thermal conductivity in superlattices : A first-principles formalism," *Physical Review B*, vol. 87, p. 140302, 2013.

[112] J. Garg, N. Bonini, B. Kozinsky, and N. Marzari, "Role of disorder and anharmonicity in the thermal conductivity of silicon-germanium alloys: a first-principles study.," *Physical Review Letters*, vol. 106, p. 045901, Jan. 2011.

[113] N. Bonini, J. Garg, and N. Marzari, "Acoustic phonon lifetimes and thermal transport in free-standing and strained graphene.," *Nano Letters*, vol. 12, p. 2673, June 2012.

[114] P. D. Robb and A. J. Craven, "Column ratio mapping: a processing technique for atomic resolution high-angle annular dark-field (HAADF) images.," *Ultramicroscopy*, vol. 109, pp. 61–69, Dec. 2008.

[115] D. Bimberga, D. Mars, J. N. Miller, R. Bauer, D. Oertel, and J. Christen, "Kinetics of Island Formation at the Interfaces of AlGaAs/GaAs/AlGaAs Quantum Wells upon Growth Interruption," *Superlattices and Microstructures*, vol. 3, no. 1, pp. 79–82, 1987.

[116] F. Hofmann, J. Garg, A. A. Maznev, A. Jandl, M. Bulsara, E. A. Fitzgerald, G. Chen, and K. A. Nelson, "Intrinsic to extrinsic phonon lifetime transition in a gaas–alas superlattice," *Journal of Physics: Condensed Matter*, vol. 25, no. 29, p. 295401, 2013.

[117] C. Colvard, R. Merlin, M. V. Klein, and A. Gossard, "Observation of Folded Acoustic Phonons in a Semiconductor Superlattice," *Physical Review Letters*, vol. 45, no. 4, pp. 298–301, 1980.

[118] J. Wang, Y. Hashimoto, J. Kono, A. Oiwa, H. Munekata, G. Sanders, and C. Stanton, "Propagating coherent acoustic phonon wave packets in $\mathrm{In}_x\mathrm{Mn}_{1-x}\mathrm{As}/\mathrm{GaSb}$," *Physical Review B*, vol. 72, p. 153311, Oct. 2005.

[119] S. Motoyama, Y. Ichikawa, Y. Hiwatari, and A. Oe, "Molecular dynamics calculation of the thermal conductivity of superlattices," *Physical Review B*, vol. 66, p. 024301, June 2002.

[120] R. Landauer, "Electrical resistance of disordered one-dimensional lattices," *Philosophical Magazine*, vol. 21, pp. 863–867, 1970.

[121] B. Gundrum, D. Cahill, and R. Averback, "Thermal conductance of metal-metal interfaces," *Physical Review B*, vol. 72, pp. 1–5, Dec. 2005.

[122] A. J. Minnich, G. Chen, S. Mansoor, and B. S. Yilbas, "Quasiballistic heat transfer studied using the frequency-dependent Boltzmann transport equation," *Physical Review B*, vol. 84, p. 235207, Dec. 2011.

[123] M. A. Afromowitz, "Thermal conductivity of $\mathrm{Ga}_{1-x}\mathrm{Al}_x\mathrm{As}$ alloys," *Journal of Applied Physics*, vol. 44, no. 3, p. 1292, 1973.

[124] E. Landry and A. McGaughey, "Effect of interfacial species mixing on phonon transport in semiconductor superlattices," *Physical Review B*, vol. 79, pp. 29–34, Feb. 2009.

[125] S. Baroni, P. Giannozzi, and A. Testa, "Green's-function approach to linear response in solids," *Physical Review Letters*, vol. 58, pp. 1861–1864, May 1987.

[126] K. Esfarjani, G. Chen, and H. T. Stokes, "Heat transport in silicon from first principles calculations," *Physical Review B*, vol. 84, pp. 1–11, Aug. 2011.

[127] G. Deinzer, G. Birner, and D. Strauch, "Ab initio calculation of the linewidth of various phonon modes in germanium and silicon," *Physical Review B*, vol. 67, pp. 1–6, Apr. 2003.

[128] S. Hepplestone and G. Srivastava, "Theory of interface scattering of phonons in superlattices," *Physical Review B*, vol. 29, pp. 3138–3147, Oct. 2010.

[129] S.-i. Tamura, "Isotope scattering of dispersive phonons in Ge," *Physical Review B*, vol. 27, no. 2, pp. 858–866, 1983.

[130] B. Abeles, "Lattice Thermal Conductivity of Disordered Semiconductor Alloys at High Temperatures," *Physical Review*, vol. 131, pp. 1906–1911, Sept. 1963.

[131] B. N. Kamitakahara, W. A., Brockhouse, "Vibrations of a mixed crystal: neutron scattering from $Ni_{55}Pd_{45}$," *Physical Review B*, vol. 10, no. 4, pp. 1200–1212, 1973.

[132] K. Esfarjani and H. Stokes, "Method to extract anharmonic force constants from first principles calculations," *Physical Review B*, vol. 77, pp. 1–7, Apr. 2008.

[133] H. J. Monkhorst and J. D. Pack, "Special points for Brillouin-zone integrations," *Physical Review B*, vol. 13, no. 12, pp. 5188–5192, 1976.

[134] A. D. Corso, S. Baroni, R. Resta, and S. de Gironcoli, "Ab iniitio calculation of phonon dispersion in II-VI semiconductors," *Physical Review B*, vol. 47, no. 7, pp. 3588–3592, 1993.

[135] D. S. Lee, Patrick A., Fisher, "Anderson Localization in Two Dimensions," *Physical Review Letters*, vol. 47, no. 12, pp. 882–885, 1981.

[136] C. Caroli, R. Combescot, P. Nozieres, and D. Saint-James, "Direct calculation of the tunneling current," *Journal of Physics C Solid State Physics*, vol. 4, no. 8, pp. 916–929, 1971.

[137] N. S. Meir, Yigal, Wingreen, "Landauer Formula for the Current through an Interacting Electron Region," *Physical Review Letters*, vol. 68, no. 16, pp. 2512–2515, 1992.

[138] M. P. L. Sancho, J. M. L. Sancho, and J. Rubio, "Quick iterative scheme for the calculation of transfer matrices: application to Mo (100)," *Journal of Physics F Metal Physics*, vol. 14, no. 5, pp. 1205–1215, 1984.

[139] M. P. L. Sancho, J. M. L. Sancho, J. M. L. Sancho, and J. Rubio, "Highly convergent schemes for the calculation of bulk and surface Green functions," *Journal of Physics F Metal Physics*, vol. 15, no. 4, pp. 851–858, 1985.

[140] G. Pernot, M. Stoffel, I. Savic, F. Pezzoli, P. Chen, G. Savelli, A. Jacquot, J. Schumann, U. Denker, I. Mönch, C. Deneke, O. G. Schmidt, J. M. Rampnoux, S. Wang, M. Plissonnier, A. Rastelli, S. Dilhaire, and N. Mingo, "Precise control of thermal conductivity at the nanoscale through individual phonon-scattering barriers.," *Nature Materials*, vol. 9, pp. 491–495, June 2010.

[141] R. M. Costescu, D. G. Cahill, F. H. Fabreguette, Z. A. Sechrist, and S. M. George, "Ultra-low thermal conductivity in W/Al_2O_3 nanolaminates," *Science*, vol. 303, pp. 989–90, Feb. 2004.

[142] C. Chiritescu, D. G. Cahill, N. Nguyen, D. Johnson, A. Bodapati, P. Keblinski, and P. Zschack, "Ultralow thermal conductivity in disordered, layered WSe_2 crystals.," *Science*, vol. 315, pp. 351–353, Jan. 2007.

[143] S. C. Huberman, J. M. Larkin, A. J. H. McGaughey, and C. H. Amon, "Disruption of superlattice phonons by interfacial mixing," *Physical Review B*, vol. 88, p. 155311, Oct. 2013.

[144] Y. S. Ju and K. E. Goodson, "Phonon scattering in silicon films with thickness of order 100 nm," *Applied Physics Letters*, vol. 74, p. 3005, May 1999.

[145] Y. Hu, L. Zeng, A. J. Minnich, M. S. Dresselhaus, and G. Chen, "Spectral mapping of thermal conductivity through nanoscale ballistic transport.," *Nature nanotechnology*, June 2015.

[146] L.-D. Zhao, S.-H. Lo, Y. Zhang, H. Sun, G. Tan, C. Uher, C. Wolverton, V. P. Dravid, and M. G. Kanatzidis, "Ultralow thermal conductivity and high thermoelectric figure of merit in SnSe crystals.," *Nature*, vol. 508, pp. 373–7, Apr. 2014.

[147] T. C. Harman, P. J. Taylor, M. P. Walsh, and B. E. LaForge, "Quantum dot superlattice thermoelectric materials and devices.," *Science (New York, N.Y.)*, vol. 297, pp. 2229–32, Sept. 2002.

[148] M. Maldovan, "Phonon wave interference and thermal bandgap materials," *Nature Materials*, vol. 14, pp. 667–674, June 2015.

[149] C. L. Tien and G. Chen, "Challenges in Microscale Conductive and Radiative Heat Transfer," *Journal of Heat Transfer*, vol. 116, p. 799, Nov. 1994.

[150] D. L. Nika, A. I. Cocemasov, D. V. Crismari, and A. A. Balandin, "Thermal conductivity inhibition in phonon engineered core-shell cross-section modulated Si/Ge nanowires," *Applied Physics Letters*, vol. 102, p. 213109, May 2013.

[151] Y. Wang, H. Huang, and X. Ruan, "Decomposition of coherent and incoherent phonon conduction in superlattices and random multilayers," *Physical Review B*, vol. 90, p. 165406, Oct. 2014.

[152] J. Ravichandran, A. K. Yadav, R. Cheaito, P. B. Rossen, A. Soukiassian, S. J. Suresha, J. C. Duda, B. M. Foley, C.-H. Lee, Y. Zhu, A. W. Lichtenberger, J. E. Moore, D. A. Muller, D. G. Schlom, P. E. Hopkins, A. Majumdar, R. Ramesh, and M. A. Zurbuchen, "Crossover from incoherent to coherent phonon scattering in epitaxial oxide superlattices.," *Nature materials*, vol. 13, pp. 168–172, Dec. 2013.

[153] D. O. Klenov, D. C. Driscoll, A. C. Gossard, and S. Stemmer, "Scanning transmission electron microscopy of ErAs nanoparticles embedded in epitaxial $In_{0.53}Ga_{0.47}As$ layers," *Applied Physics Letters*, vol. 86, p. 111912, Mar. 2005.

[154] C. Kadow, S. B. Fleischer, J. P. Ibbetson, J. E. Bowers, A. C. Gossard, J. W. Dong, and C. J. Palmstrøm, "Self-assembled ErAs islands in GaAs: Growth and subpicosecond carrier dynamics," *Applied Physics Letters*, vol. 75, p. 3548, Nov. 1999.

[155] P. Chen, N. A. Katcho, J. P. Feser, W. Li, M. Glaser, O. G. Schmidt, D. G. Cahill, N. Mingo, and A. Rastelli, "Role of Surface-Segregation-Driven Intermixing on the Thermal Transport through Planar Si / Ge Superlattices," *Physical Review Letters*, vol. 111, p. 115901, Sept. 2013.

[156] W. Kim, S. L. Singer, A. Majumdar, D. Vashaee, Z. Bian, A. Shakouri, G. Zeng, J. E. Bowers, J. M. O. Zide, and A. C. Gossard, "Cross-plane lattice and electronic thermal conductivities of ErAs:InGaAsâĹȚInGaAlAs superlattices," *Applied Physics Letters*, vol. 88, p. 242107, June 2006.

[157] M. L. Lee and R. Venkatasubramanian, "Effect of nanodot areal density and period on thermal conductivity in SiGe/Si nanodot superlattices," *Applied Physics Letters*, vol. 92, p. 053112, Feb. 2008.

[158] D. S. Wiersma, P. Bartolini, A. Lagendijk, and R. Righini, "Localization of light in a disordered medium," vol. 390, pp. 671–673, Dec. 1997.

[159] P. Sheng, *Introduction to Wave Scattering, Localization and Mesoscopic Phenomena.* New York: Springer Berlin Heidelberg, second edition ed., 2006.

[160] P. W. Anderson, "Absence of Diffusion in Certain Random Lattices," *Physical Review*, vol. 109, pp. 1492–1505, Mar. 1958.

[161] S. John, "Strong localization of photons in certain disordered dielectric superlattices," *Physical Review Letters*, vol. 58, pp. 2486–2489, June 1987.

[162] P. Sheng, X. Zhang, Z. Liu, and C. Chan, "Locally resonant sonic materials," *Physica B: Condensed Matter*, vol. 338, pp. 201–205, Oct. 2003.

[163] R. Venkatasubramanian, "Lattice thermal conductivity reduction and phonon localizationlike behavior in superlattice structures," *Physical Review B*, vol. 61, pp. 3091–3097, Jan. 2000.

[164] J. H. Page, P. Sheng, H. P. Schriemer, I. Jones, X. Jing, and D. A. Weitz, "Group Velocity in Strongly Scattering Media," *Science*, vol. 271, pp. 634–637, Feb. 1996.

[165] J. E. Graebner, B. Golding, and L. C. Allen, "Phonon localization in glasses," *Physical Review B*, vol. 34, pp. 5696–5701, Oct. 1986.

[166] J. E. Graebner and B. Golding, "Phonon localization in aggregates," *Physical Review B*, vol. 34, pp. 5788–5790, Oct. 1986.

[167] A. F. Ioffe and A. R. Regel, "Non-crystalline, amorphous and liquid electronic semiconductors," *Prog. Semicond*, vol. 4, pp. 237–291, 1960.

[168] Z. Tian, K. Esfarjani, and G. Chen, "Green's function studies of phonon transport across Si/Ge superlattices," *Physical Review B*, vol. 89, p. 235307, June 2014.

[169] Y. Koh and D. Cahill, "Frequency dependence of the thermal conductivity of semiconductor alloys," *Physical Review B*, vol. 76, p. 075207, Aug. 2007.

[170] A. J. Minnich, J. A. Johnson, A. J. Schmidt, K. Esfarjani, M. S. Dresselhaus, K. A. Nelson, and G. Chen, "Thermal conductivity spectroscopy technique to measure phonon mean free paths," *Physical Review Letters*, vol. 107, p. 095901, Aug. 2011.

[171] M. N. Luckyanova, J. A. Johnson, A. Maznev, J. Garg, A. Jandl, M. T. Bulsara, E. A. Fitzgerald, K. A. Nelson, and G. Chen, "Anisotropy of the Thermal Conductivity in GaAs/AlAs Superlattices," *Nano Letters*, vol. 13, no. 9, pp. 3973–3977, 2013.

[172] L. L. Chang, "The Growth of a GaAs-GaAlAs Superlattice," *Journal of Vacuum Science and Technology*, vol. 10, p. 11, Jan. 1973.

[173] R. B. Wilson and D. G. Cahill, "Anisotropic failure of Fourier theory in time-domain thermoreflectance experiments.," *Nature communications*, vol. 5, p. 5075, Jan. 2014.

[174] D. Ding, X. Chen, and A. J. Minnich, "Radial quasiballistic transport in time-domain thermoreflectance studied using Monte Carlo simulations," *Applied Physics Letters*, vol. 104, p. 143104, Apr. 2014.